Analysis of Optical Millimeter-wave Generation Using Injection-locked Semiconductor Lasers

Analysis of Optical Millimeter-wave Generation

Using Injection-locked Semiconductor Lasers

2001   6

_____

_____

_____

_____

_____

2001   6

Abstract

Analysis of Optical Millimeter-wave Generation

Using Injection-locked Semiconductor Lasers

Jung-Tae Kim

Department of Electrical and Electronic Engineering

The Graduate School

Yonsei University

The demand for new services and the increasing number of subcarrier requiring high-speed digital data transmission have pushed carrier frequencies from the microwave towards the millimeter-wave range. In broadband networks based on the inherent advantages of the millimeter-wave range, wider radio frequency channels can be allocated. Wireless connection of subscribers significantly reduces maintenance and installation costs, and allows mobile applications. However, due to the high atmospheric attenuation of millimeter-wave signals, it is straightforward to employ fiber-optic techniques when feeding many base stations.

Several methods have been reported for the optical generation of modulated RF carriers in fiber-wireless system implementation. These include optical heterodyne and self-heterodyne techniques such as dual-mode semiconductor laser and harmonic signal generating pulsed lasers. However, the simplest technique for the optical generation and distribution of the RF signal modulation is an intensity modulation scheme via direct or external modulation of a laser. Since the direct modulation suffers from the effects of laser frequency chirp, external modulator is the preferred choice in fiber-optic links.

This dissertation deals with the spectral characteristics of semiconductor lasers locked to the external light injected from a modulated laser. The numerical model for semiconductor lasers under the external optical injection is based on the Lang's equation and has been extended in order to take into account the simultaneous injection of the multiple sidebands of the current-modulated laser. The numerical simulation results show that the unselected sidebands will affect the optical and RF-spectral characteristics even when the semiconductor laser is locked to the target sidebands. The numerical analysis will help to estimate the parameter to be extracted.

_____

Acknowledgements

I would like to express my sincere gratitude to my chief advisor, Professor Woo-Young Choi, for his valuable insight, guidance, encouragement, and support throughout the course of my study at Yonsei University. I am also grateful to Professors Bong-Ryul Kim, Sang-Kook Han, Chung-Yong Lee, and Chang-Woo Hu for their advice as well.

I would also like to express my gratitude to Dr. Jong-Wook Han, Choon-Soo Kim, Professor Young-Sik Jang, who are all my ex-colleagues from ETRI(Electronics and Telecommunications Research Institute).

I really want to acknowledge members of High-speed Information Transmission Laboratory at Yonsei University and, in particular, Dr. Kyung-Hwan Kim, Mr. Young-Kwang Seo, You-Gun Kim, and Jae-Wook Lee for their excellent assistance.

My special thanks go to two of my colleagues at Tongwon College. One is Professor Kwinam Mun who proofread my dissertation for any mistakes and the other is Professor Ik-Tae Uhm who offered valuable comments. I also want to thank all of my department colleagues and everybody who helped me at Tongwon College.

Finally, I would like to convey my utmost gratitude to Tongwon College President, Dr. Jung-Eun Lee for her constant support.

I'd like to dedicate this dissertation to my dear wife, Hyang-Mi Kim, who has been patient and understanding throughout the course of this endeavor and to my lovely son, Dong-Koo Kim and daughter, Sung-Eun Kim, and to my parents, brothers, and the family of my wife.

Table of Contents

List of Figures

List of Tables

Chapter 1. Introduction

Design of broadband access networks to deliver services such as video-on-demand, interactive multimedia, high-speed internet, and high-density television to homes and industrial and educational institutions has been a subject of intense interest in recent years. Both wireline, hybrid fiber-coax (HFC) and wireless [Local Multi-point Distribution System (LMDS)] access techniques show considerable potential in this regard. These access schemes mainly utilize the lower microwave frequency spectrum (<5 GHz) for distribution of broadband signals. Recently, however, the millimeter-wave frequency band (26~60 GHz) has been considered for wireless access, primarily to avoid spectral congestion at lower microwave frequencies and to offer large transmission bandwidth. Future millimeter-wave broadband access systems may employ an architecture in which signals generated at a central location will be transported to remote base stations for wireless distribution [1, 2]. Optical feeding of base stations in these systems is an attractive approach because it enables a large number of base stations to share the transmitting and processing equipments remotely located from the customer serving area.

In such systems, millimeter-wave signals can be generated and modulated using optical techniques and transported to base stations very efficiently via low cost, low loss, and EMI-free optical fibers. Together with high-speed photodetectors integrated with mixer, amplifiers, diplexers and printed

antennas, simple and lightweight base stations can be designed to allow easy installation on building walls and corners, street lights, and telephone poles.

Figure 1-1 shows a basic configuration of a pico-cellular mobile communication system using optical techniques for the generation and transmission of millimeter-wave signals. A number of techniques for the generation, modulation, and distribution of millimeter-wave modulated optical carriers for fiber-wireless systems have been developed [3]. Optical millimeter-wave generated, in particular, has been attracting much attention in applications for broadband wireless systems, coherent multi-frequency optical communications and optical beam forming because of its flexibility in generating various frequencies. Optical sideband injection locking is one technique for its implementation. When a semiconductor laser (Master Laser) is current-modulated, it is simultaneously intensity-modulated and frequency modulated due to its frequency chirp, so that it produces a broad sideband in optical spectrum. The millimeter-wave signals can be obtained when two slave lasers are injection-locked to two different target sidebands of the master laser. When CW (Continuous Waveform) light from the master laser is injected into the slave laser, the slave laser typically shows the distinguishable spectral behaviors : unlocking, dynamically stable locking, and dynamically unstable locking. When slave laser is injection-locked to target FM (Frequency Modulation) sideband of current-modulated laser, its spectral behaviors are different from those of CW injection-locked slave lasers due to the existence of the unselected other sidebands of the master laser.

This dissertation deals with the influence of multiple sidebands from master laser on the spectral characteristics of sidebands injection-locked semiconductor lasers numerically.

This dissertation is organized as follows. In Chapter 2, techniques for optical millimeter-wave generation are introduced and explained in detail. In chapter 3, we recall the basics of the optical injection locking. In chapter 4, we calculate power spectra corresponding to different injection locking regimes and analyze the spectral characteristics of semiconductor.
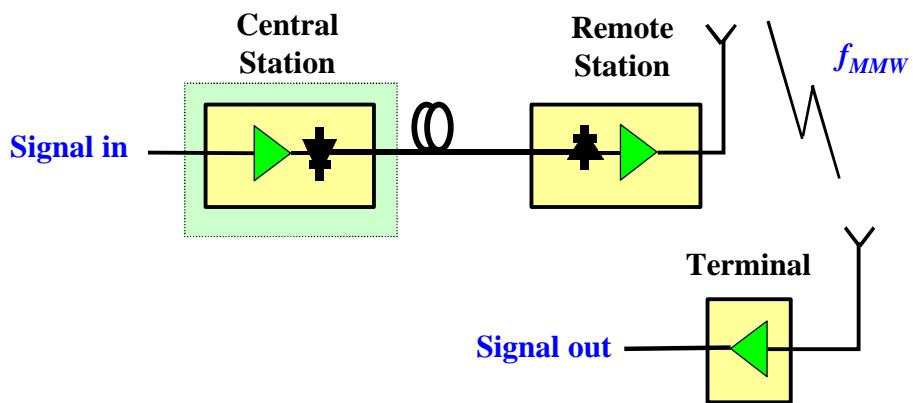
Fig. 1-1. Application of wireless fiber-optic communication using

millimeter-wave signal

Chapter 2. Techniques for Optical Millimeter-wave Generation

A fiber-optic millimeter-wave uplink system can be classified as baseband , microwave IF (Intermediate Frequency) subcarrier and millimeter-wave radio frequency subcarrier according to subcarrier frequencies of signals transmitted in an optical fiber link. In the baseband transmission, influence of the fiber dispersion effect is negligible, and the base station configuration is the most complex. To use this method without a subcarrier frequency, it has no choice but to adopt time-division or code-division multiplexing. This requires higher-speed electrical processors. In the IF subcarrier transmission, the fiber dispersion effect does not cause a serious problem. Subcarrier miltiplexing can be employed, but downconversion from a millimeter-wave to an IF band is required at the base station. In the RF (Radio Frequency) subcarrier transmission, the base station configuration can be simplified only if a millimeter-wave optical external modulator and a high-frequency photodiode are respectively applied to the electric-to-optic (E/O) and the optic-to-electric (O/E) converters. For a simple base station configuration the millimeter-wave optical external modulation technique will be one of the best solutions [4].

A basic configuration is shown in Fig. 2-1(c). It consists of millimeter-wave link by using fiber-optic to deliver millimeter-wave signal transmission technique. Data transmitted in central station through millimeter-wave link is transmitted into base station by using fiber-optic link. And, it spreads out by

wireless data through the antenna in base station. A fiber-optic millimeter-wave system can be classified as baseband, IF subcarrier and millimeter-wave radio frequency subcarrier. In baseband configuration, a signal in control station is transmitted into base station through fiber link. The transmitted signal is upconverted to an IF band signal. IF signal is modulated with LO (Local Oscillator) generating millimeter-wave frequency and transmitted into air by an antenna. This method is very difficult to handle because of complexity of base station. IF subcarrier configuration is shown in Fig. 2-1(b), the signal is transmitted after modulating with IF baseband in control station. Then signal is upconverted to millimeter-wave with local oscillator in base station. Compared to baseband system, the base station is simpler. In millimeter-wave radio frequency subcarrier system, it is possible for the base station to consist of only three simple components : a photodiode, millimeter-wave amplifier, and millimeter-wave antenna. This system has two advantages in leading to a simple base station configuration. One is that no millimeter-wave sources are required at the base station. The other is that no millimeter-wave mixer is needed [5].

Central station   **Base station**

(a)

(b)

(c)
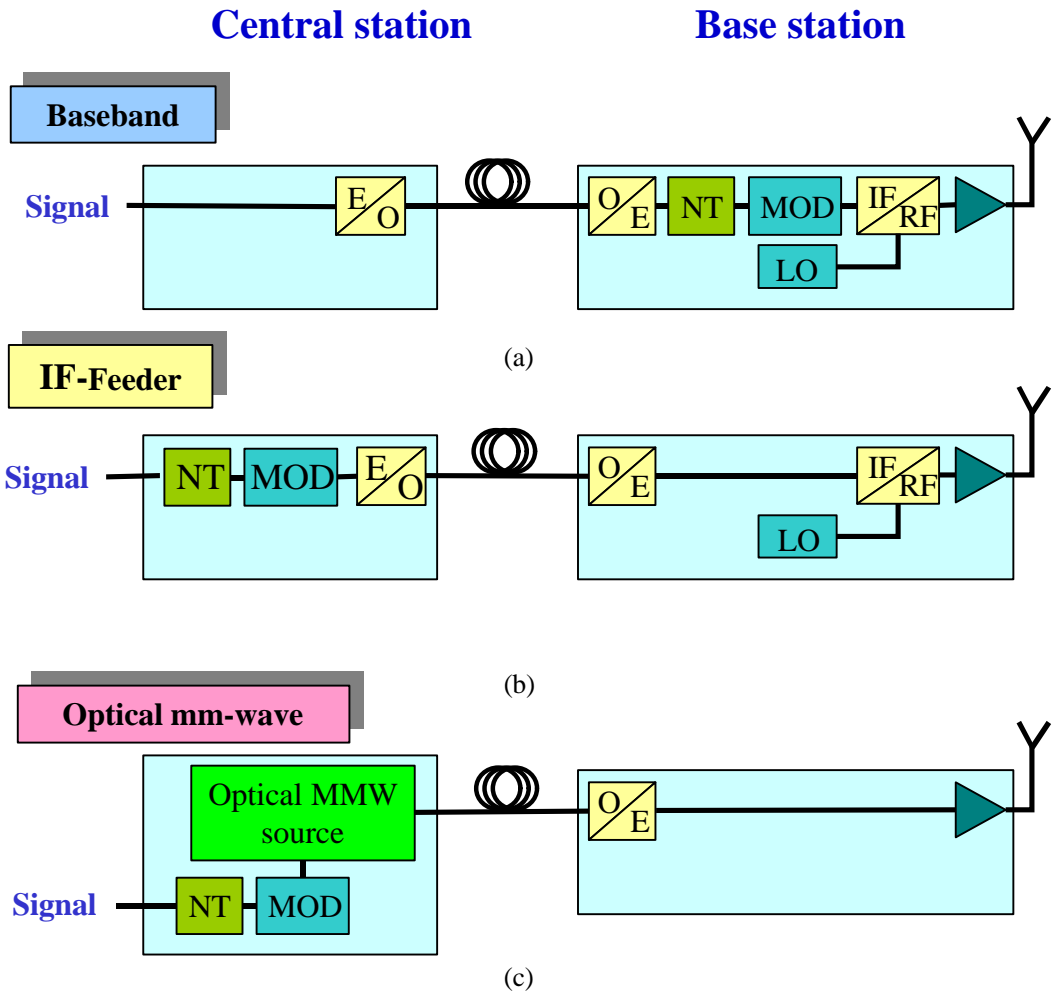
NT : Network Terminal, MOD : Modulator, LO : Local Oscillator

IF : Intermediate frequency, RF : Radio frequency

E/O : Electrical to Optical, O/E : Optical to Electrical

Fig. 2-1. Millimeter-wave link using fiber-optic configuration

2.1 Systems Using Intensity Modulation Direct Detection Technique

2.1.1 Direct or External Intensity Modulation

Fiber-optic microwave and millimeter-wave links which are subject to a still increasing interest can be implemented either by the use of direct detection techniques or heterodyne detection techniques. Many such links have been proposed, analyzed, and experimented. In the direct detection, the millimeter-wave signal is intensity modulated onto the optical carrier from a laser. The optical signal is then transmitted through the optical fiber, and the millimeter-wave signal is recovered by direct detection in a photodiode. In the remote heterodyne detection links, two phase correlated optical carriers are generated in a dual-frequency laser transmitter with a frequency offset the same as to the desired millimeter-wave frequency. Further, one of the optical carriers is modulated by the information to be contained in the millimeter-wave signal. Both optical signals are then transmitted through the optical fiber, and the millimeter-wave signal is generated by heterodyning the two optical signals in a photodiode. In both approaches the chromatic fiber dispersion becomes a limiting factor for the transmission distance when the microwave signals are in the above 20 GHz regime.

In an Intensity Modulation Direct Detection link (IMDD), the millimeter-wave signal is carried as a lower and upper sideband on the optical carrier. Due to the dispersion and the large frequency offset between the side bands

and the optical carrier, the phase of each of the spectral components of the transmitted optical signal has experienced a differential change. After detection, this results in a power reduction of the recovered millimeter-signal and thereby decreasing its carrier to noise ratio (CNR). The dispersion induced CNR penalty on the recovered millimeter-wave signal with the carrier frequency is found by comparing the signal power of millimeter-wave signal which is recovered by square law detection of the optical signal. Power shift of millimeter-wave signal is characterized by function of fiber distance due to the chromatic dispersion effect in fiber. IM-DD link and shift of optical spectrum by external modulation technique is shown in Fig. 2-2. Power shift is induced by a dispersion limited fiber length and is represented as follows [6].

$$P_c = \cos\left[\left(\frac{lLD}{c}\right)l^2 f_{MMW}^2\right] \tag{2-1}$$

where f_{MMW} denotes the RF offset frequency from the optical carrier, l is the optical wavelength, L is the length of fiber, D is the chromatic dispersion parameter and c is the speed of light in vacuum. As shown in Fig. 2-3, for a millimeter-wave of 30 GHz and 60 GHz, the dispersion results in a significant decrease of the CNR as the transmission distance is increased. CNR penalty is defined as follows.

$$CNR_{penalty} = 10\log\left[\frac{P_{c\,without\,dispersion}}{P_{c\,with\,dispersion}}\right] \tag{2-2}$$

This penalty limits the obtainable transmission in IM-DD fiber-optic millimeter-wave links. A complete extinction of the recovered millimeter-wave carrier occurs when the lower and upper sidebands are out of phase. The millimeter-wave carrier at 30 GHz is transmitted on an optical carrier at a wavelength of 1550 nm over a standard single-mode fiber with a chromatic dispersion of 17 ps/km·nm, large CNR penalty occurs for a transmission distance of 4 km. Furthermore, from Fig. 2-3, it is seen that the dispersion effect exhibits a cyclic behavior. The period length is found from the following equation [7].

$$\Delta L = \frac{c}{D\lambda^2 f_{MMW}^2} \tag{2-3}$$

The dependence of transmission of distance on chromatic fiber dispersion and millimeter-wave frequency can be estimated above equation. An increase in either dispersion or carrier frequency, therefore, significantly limits the obtainable transmission distance.

MMW Source + Data

LD   Modulator   Optical Fiber   PD

MMW
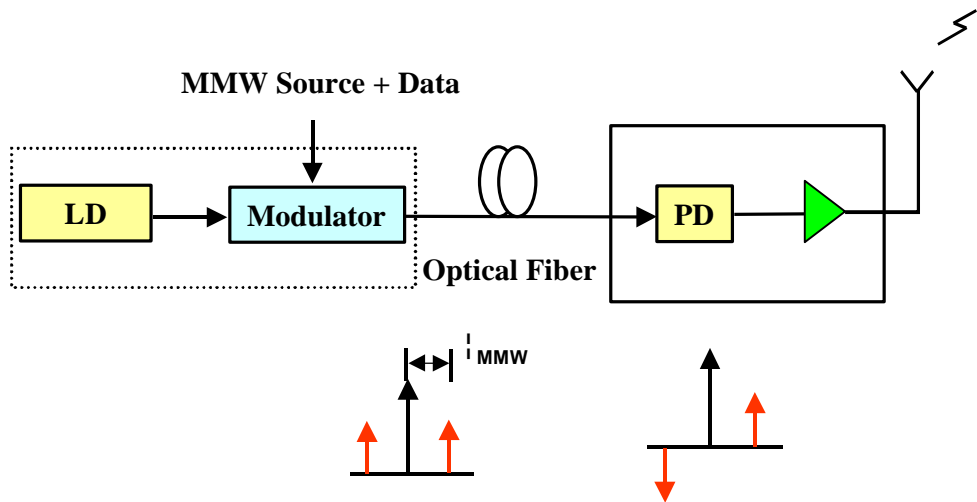
LD : Laser Diode

PD : Photo Diode

Fig. 2-2. Optical spectrum shift and IM-DD link using external modulation
method
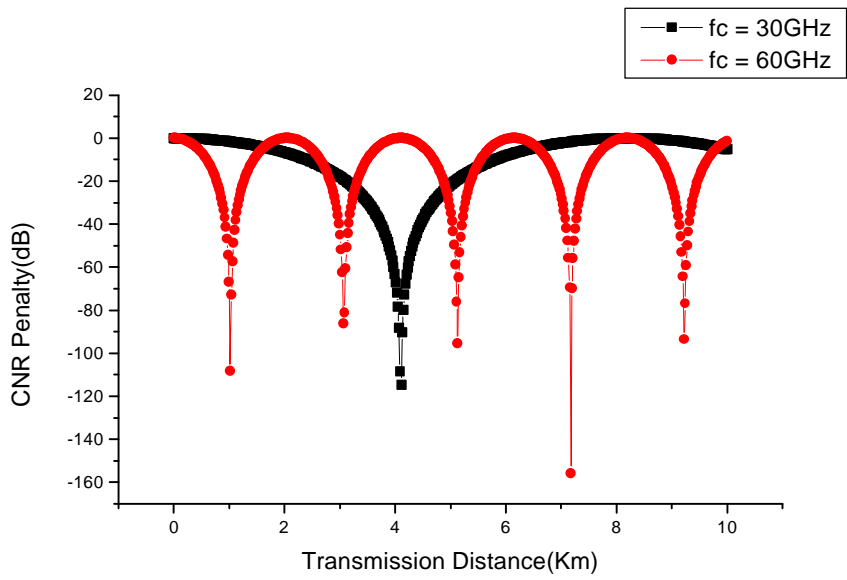
Fig. 2-3. Dispersion induced CNR penalty as a function of transmission
distance

2.2 Systems Using Heterodyne Detection Techniques

In the direct detection links, the millimeter-wave signal is intensity modulated onto the optical carrier from a laser. The optical signal is then transmitted through the optical fiber, and the millimeter-wave signal is recovered by direct detection in a photodiode. In the heterodyne links, two phase-correlated optical carriers are generated in a dual-frequency laser transmitter with a frequency offset equal to the desired millimeter-wave frequency. Both optical signals are then transmitted through the optical fiber, and the millimeter-wave signal is generated by heterodyning method of the two optical signals in a photodiode. The principles of heterodyning detection links are quite different from those of IM-DD links. The major difference is that the IM-DD link transmits the millimeter-wave signal as sidebands on a single laser signal whereas the heterodyning detection link generates the millimeter-wave signal by beating of two laser signals. In this process, the phase noise of the two laser signals transfers directly to the resulting microwave signal. Therefore, it is necessary either to remove the actual laser-signal phase noise or to correlate the phase noise of the two laser signals. Both methods or a combination ideally ensures the generation of a highly phase-stable millimeter-wave [8].

A simplified schematic of the heterodyning principle is shown in Fig. 2-4. At the transmitter end, two phase-correlated laser signals with a frequency offset of $f_c = |f_1 - f_2|$ are generated by a dual-frequency laser transmitter. Both

laser signals are transmitted through the fiber link to the receiver end where heterodyning takes place in an O/E converter (photodiode). Assuming that the phase correlation between the two laser signals is not altered by the fiber link, the resulting beat signal is a highly phase stable millimeter-wave carrier with a frequency of f_c. However, the phase correlation is altered to some extend by the fiber link which, besides transmission attenuation, may limit the system performance due to dispersion effects and fiber nonlinearities. Both chromatic dispersion and polarization-mode dispersion limit have the obtainable transmission-distance two times the millimeter-wave carrier frequency product of the link [63].

Assuming optical source is w_1 and w_2 respectively, electrical field is represented as follows [9].

$$E_1 = \sqrt{P_1}\cos[w_1 t + \Phi_1(t)] \tag{2-4}$$

$$E_2 = \sqrt{P_2}\cos[w_2 t + \Phi_2(t)] \tag{2-5}$$

Two optical sources are transmitted through fiber into photodiode and generated current component. Current is square of field and is shown in the following equation.

$$I_{PD}(t) \propto P_1 + P_2 + 2\sqrt{P_1 P_2}\cos\left[|w_2 - w_1|t - |\Phi_2(t) - \Phi_1(t)|\right] \tag{2-6}$$

I_{PD} is current of photodiode and is called beat signal. $P_1 + P_2$ is a DC

element in photodiode current, the other component is desired millimeter-wave signal. We can easily obtain millimeter-wave signal in photodiode by controlling properly to meet desired millimeter-wave frequency difference of the two optical sources. However, the phase components of the two optical sources are random and the signal linewidth generated by beating two optical sources is described as sum of two optical source linewidth which has a several MHz. When a signal with a broad width is transmitted, the overall system performance is limited because its spectral efficiency is small. To overcome this limitation, several methods are reported and proposed as follows. These techniques normally focus on generating millimeter-wave source with low phase noise and several techniques. Techniques are shown as follows.

    a. Single Sideband Modulation

    b. 2-sideband Modulation

    c. Mode locking

    d. Optical Phase Lock Loop

    e. Sideband Injection Locking
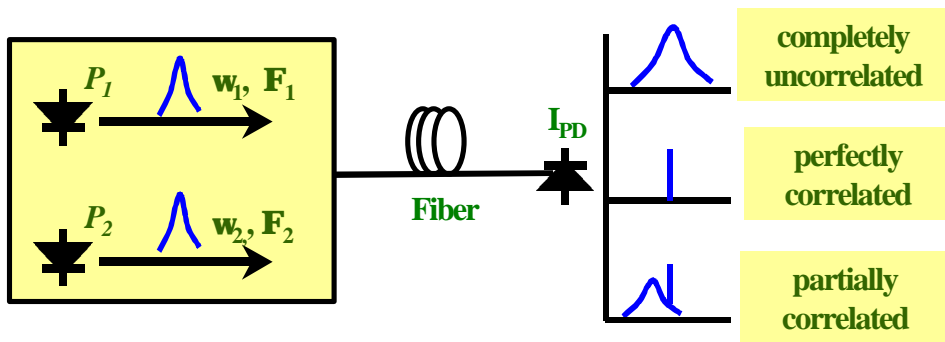
Fig. 2-4. Millimeter-wave signal gereration by optical beating scheme

2.2.1 Single Sideband Modulation Method

In conventional intensity modulation, the optical carrier is modulated to generate an optical field with a carrier and two sidebands (double-sideband (DSB) modulation). At the optical receiver, each sideband beats with the optical carrier, thereby generating two beat signals which constructively interfere to produce a single component at the RF frequency. However, if the signal is transmitted over fiber, chromatic dispersion causes each spectral component to experience different phase shifts depending on the fiber-link distance, modulation frequency, and the fiber-dispersion parameter. These phase shifts make the relative phases between the carrier and each sideband different, which can result in a power degradation as shown in Fig. 2-3. When the relative phase difference becomes π, complete cancellation of the RF signal occurs [12, 13]. As the RF frequency increases, the effect of dispersion is even more pronounced and the fiber-link distance severely limited. By using MZM (Mach Zehnder Modulator) of dual electrode, a SSB format can be obtained not by controlling a phase of modulated signal as illustrated in Fig. 2-5. Dispersion effects can be reduced further and almost totally overcome by eliminating one sideband to produce an optical carrier with single sideband (SSB) modulation. It is possible to implement millimeter-wave transmission system without having CNR penalty [14, 15].
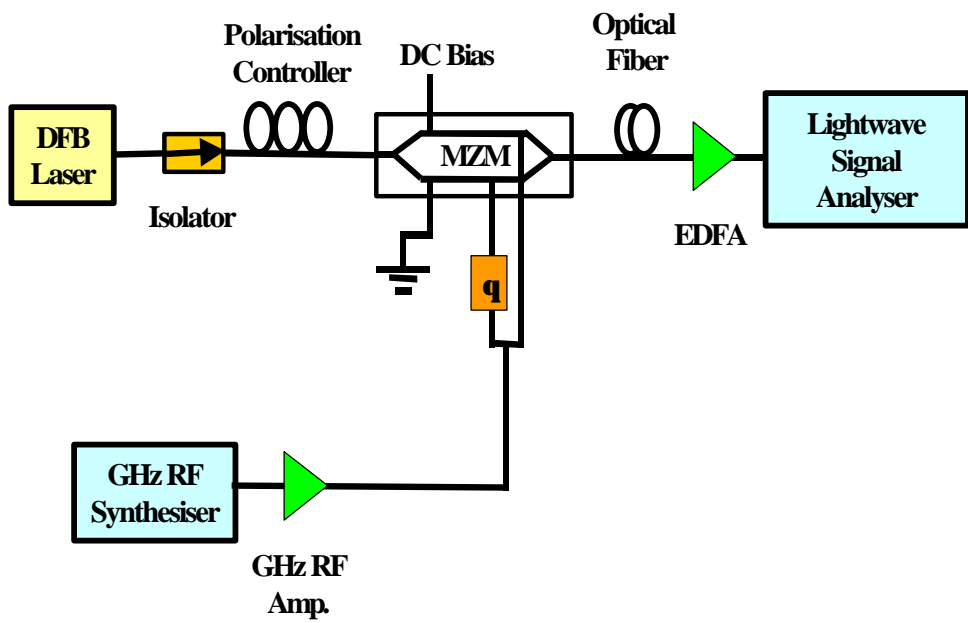
Fig. 2-5. IMDD link and optical spectrum using SSB modulation method

2.2.2 2-Side Band Modulation Method

The dual-electrode MZM can be modeled as two phase modulators in parallel, where the amplitudes of the RF drive signals applied to each electrode are equal. A continuous-wave signal from a laser with amplitude A and frequency f_c is externally modulated by an RF signal with peak-to-peak amplitude $2V_{ac}$ and frequency f_{rf}, which is split and applied to drive electrode. A phase difference of θ can exist between each drive electrode. If the modulator has a dc-bias voltage of V_{dc} on one electrode while the other dc terminal is grounded, then the output optical field is represented as follows [16].

$$E_{out}(t) = E_{in}(t)\cos(\frac{l}{2}\frac{V_{\mathrm{mod}}(t)}{V_p}) \tag{2-7}$$

where $E_{in}(t)$ in the amplitude of input optical source is injected into modulator, and $V_{\mathrm{mod}}(t)$ is a voltage to bias modulator. V_p is the switching voltage of the MZM. In the case of $V_{\mathrm{mod}}(t) = V_p(1+e) + aV_p\cos(wt)$ output field of modulator is described as follows.

$$E_{out}(t) = \cos(\frac{p}{2}[(1+e) + a\cos(wt)])\cos(\Omega t) \tag{2-8}$$

where a is the normalized amplitude of the drive signal, e is the

normalized bias and Ω is the optical carrier frequency. This equation can be expressed by a series of first order of Bessel functions as follows.

$$
\begin{aligned}
E_{out} = {} & \frac{1}{2} J_0(\boldsymbol{a}\frac{\boldsymbol{p}}{2})\cos\left(\frac{\boldsymbol{p}}{2}(1+\boldsymbol{e})\right) \\
& -\frac{1}{2} J_1(\boldsymbol{a}\frac{\boldsymbol{p}}{2})\sin\left(\frac{\boldsymbol{p}}{2}(1+\boldsymbol{e})\right)\cos(\Omega t \pm \boldsymbol{w}t) \\
& +\frac{1}{2} J_2(\boldsymbol{a}\frac{\boldsymbol{p}}{2})\cos\left(\frac{\boldsymbol{p}}{2}(1+\boldsymbol{e})\right)\cos(\Omega t \pm 2\boldsymbol{w}t) \\
& -\frac{1}{2} J_3(\boldsymbol{a}\frac{\boldsymbol{p}}{2})\sin\left(\frac{\boldsymbol{p}}{2}(1+\boldsymbol{e})\right)\cos(\Omega t \pm 3\boldsymbol{w}t)
\end{aligned}
\tag{2-9}
$$

where J_0 and J_1 are the zero and first-order Bessel functions, respectively. When $\boldsymbol{e}$ is "0", and dc component is V_p and center carrier components disappear. A power spectrum consists of an optical carrier at $\boldsymbol{w}$ and $3\boldsymbol{w}$, with DSB modulation showing components at $\boldsymbol{w}$ and $3\boldsymbol{w}$. $(\Omega \pm \boldsymbol{w})$ component is mainly shown in spectrum. We can obtain $2\boldsymbol{w}$ or $4\boldsymbol{w}$ components away from reference. The millimeter-wave signal can be obtained using an electrical VCO (Voltage Control Oscillator) at half frequency of the desired millimeter-wave frequency. This technique has an advantage, that is, chromatic dispersion problem does not occur compared to the intensity modulation direct detection because this technique has no center carrier components.

2.2.3 Mode locking Method

The generation of high-frequency signals using semiconductors has been attracting attentions in recent years due to its important role in high-speed optical communications and microwave photonic systems. High-frequency signals can be generated by a variety of techniques including gain switching, active mode locking, passive mode locking and hybrid mode locking of the semiconductors. Among these methods, the passive mode locking technique is particularly attractive because it can generate millimeter-wave signals at frequencies over 100 GHz without the limitations imposed by the available drive electronics. Its inherent drawbacks of large phase-noise and difficulty in synchronization with external circuits can be overcome by implementing stabilization schemes such as sub-harmonic optical or electrical injection techniques. Mode locking method is not a form of velocity in continuous wave laser but a pulse of millimeter-wave signal by fixing a phase of a variety of optical mode laser. We can obtain desired millimeter-wave signal by beating a frequency in photodiode after choosing two modes with desired frequency difference among synchronized modes. We briefly explain a heterodyning technique by using mode-locking method [17-19]. In Fig. 2-6, we can select desired mode by using an optical filter like Fabry-Perot filter.

In general, there are two methods to implement Mode locking scheme. One is active and the other is passive mode locking method. Active mode locking method is modulated with laser gain by injecting electrical signal to laser with

frequency in contrast to resonance of laser and is synchronized a phase with resonance mode of laser. In the contrary, passive mode lock method is synchronized with resonance mode in laser to meet a phase by putting saturable absorber. To generate a millimeter-wave frequency with this method, we have to make a passive mode lock laser for generating a light of desired frequency interval by controlling interval of resonance mode and situation of saturable absorber. Recently this technique was used in combination with a double modulation format for the transmission of 155 Mbit/s data signals at 62.9 GHz carrier frequency. But passive-lock technique is not stable in phase synchronization, recently synchronized harmonic frequency mode locking with laser diodes through optical pulse train injection and synchronization of sub-terahertz optical pulse train from PLL controlled pulse mode locked semiconductor laser is reported [20, 21].
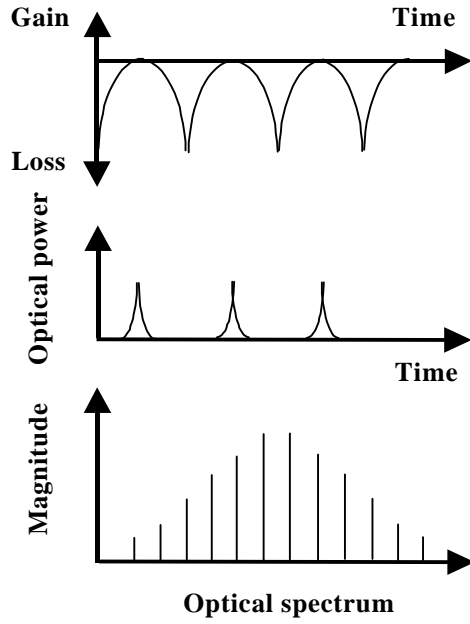
(a) passive mode-lock method
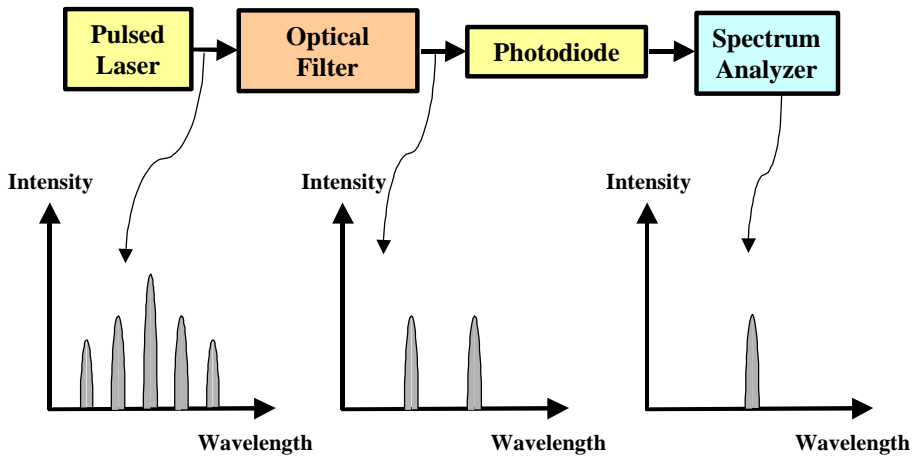
(b) generation of desired frequency

Fig. 2-6. Millimeter-wave generation using mode locking method

2.2.4 Optical Phase Lock Loop Method

OPLL (Optical Phase Lock Loop) uses a feedback circuit to synchronize two optical signals by keeping a phase of two optical sources. We describe a basic diagram of millimeter-wave generation by using OPLL method in Fig. 2-7. In this technique, we make an optical signal with a desired difference of frequency by using two lasers and compare with a stable signal originated from external reference frequency and a beating signal of two optical signals. It can synchronize two lasers by controlling an operating current of VCO (Voltage Controlled Oscillator) using a feedback signal after detecting a difference of phase through loop filter. Its basic operation is the same as electrical method except laser is used like electrical oscillator. By using this technique, we can get a stable millimeter-wave beat signal with low phase noise, although it is difficult to implement this technique. There are two important parameters, one is operating bandwidth of feedback circuit, the other is loop delay. To implement a stable OPLL mechanism, it is necessary that bandwidth of feedback circuit is very large and loop delay is small. To realize this technique, we need a small linewidth of laser and should integrate a function of major characteristics of OPLL in a small package. It is reported that a packaged semiconductor laser optical phase-locked loop for photonic generation and the processing and transmission of microwave signals are operating in 7-14 GHz [22, 23].
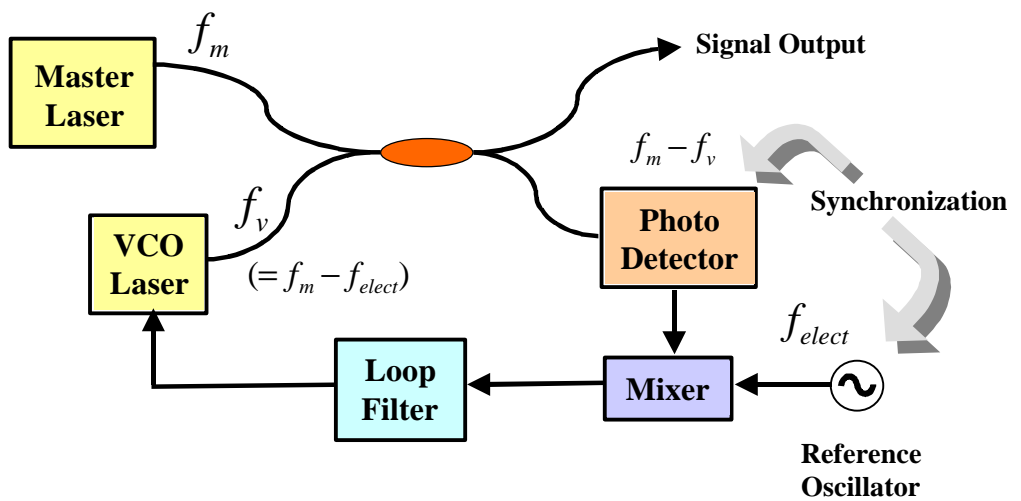
VCO : Voltage-Controlled Oscillator

Fig. 2-7. Millimeter-wave generation using OPLL method

2.2.5 Sideband Injection Locking Method

If master laser is modulated with the sub-harmonic of the desired millimeter-wave band frequency, we can see lots of sidebands generated with difference of modulation frequency in optical spectrum of master laser in Fig. 2-8. Two sidebands with desired millimeter-wave frequency differences are injected into slave lasers and lock them. These two slave lasers beat each other in photodiode and generate the desired millimeter-wave signal with low phase noise since they are synchronized by the same Master laser. Therefore, this technique is not affected by chromatic dispersion in fiber. We summarize a technique of generating a millimeter-wave signal optically in Table 1.
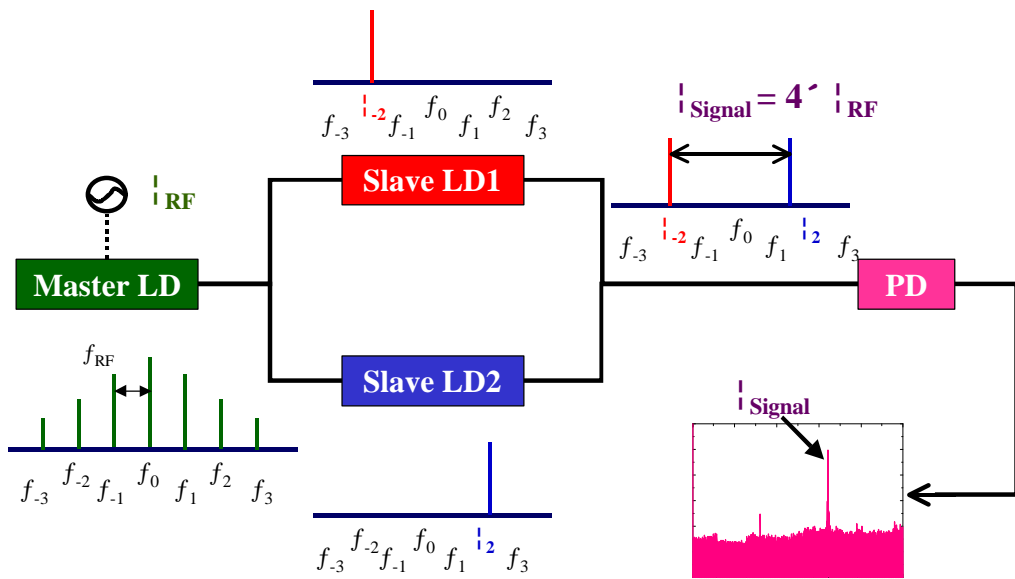
Fig. 2-8. Millimeter-wave generation using sideband injection locking
method

Table 1. Characteristics comparison of millimeter-wave generation using heterodyne method

Method	Dispersion problem	Electrical Source (>10GHz)
SSB modulation	None	f_{MMW}
2-side band modulation	None	$f_{MMW} / 2$
Mode-locking	A Little	Useless
OPLL	None	Useful (Reference OSC.)
Sideband injection locking	None	Useless

Chapter 3. Optical Injection Locking Technique

3.1 Principle of Injection Locking

Although the direct current modulation of semiconductor lasers is simple and compact, it is not suitable to the high-speed applications. It is because the lasing frequency-shift, or chirp, during the direct current modulation combined with the fiber dispersion, causes the system performance degradation. This degradation becomes more serious when the transmission speed increases. One method of overcoming the chirp and subsequent fiber dispersion problems is to use optical injection locking (OIL). OIL provides such advantages such as the reduction of chirp, linewidth, and noise [27, 28], modulation bandwidth enhancement [30], and other functions such as wavelength conversion [29], and optical generation of millimeter-wave signals [31]. Fiber-optic transmission experiments using OIL technique has been successfully demonstrated in the modulation speed less than 500 Mbps [32], but not much analytical work has been done over the effect of optical injection on transmission performance.

The optical injection locking technique with semiconductor laser diodes is widely used in chirp and linewidth reduction [34], measurement of the laser dynamics [35], wavelength conversion, and optical microwave generation. In particular, the optical microwave signal generation technique with injection locked lasers is very promising for many applications because it can easily

produce high frequency signals with low phase noise. In the sideband injection-locking scheme, the master laser (ML) is electrically modulated and two of the resulting sidebands having the desired frequency separation are injected into two slave lasers (SLs). When these two injection-locked SLs beat each other in the photodiode (PD), the desired microwave signal is generated. Using this method, Braun *et al*. has recently reported the successful demonstration of 60 GHz beat signal generation [36, 37].

Our recent study on FM sideband injection locking has shown that when SLs are locked to the target sidebands of the directly modulated ML, the presence of the unselected sidebands influences the resulting microwave signals. The unselected sidebands can produce the unwanted beat signals around the desired beat signal, which degrade the overall system performance. The reduction in the incident light power helps in suppressing the unwanted beat signals, but it also reduces the locking range causing the stability problem. Figure 3-1 (a) shows the optical spectra of OIL generated in difference between ML and SL. Optical spectra and comparison of wavelength by OIL scheme is shown in Fig. 3-1 (b). $\Delta\lambda$ is the value of difference between ML and SL wavelength.

(a) Optical spectra

$Dl = l$ (ML) - l (SL) = 0.078 nm

•Injection-locking

•SL only

•ML only
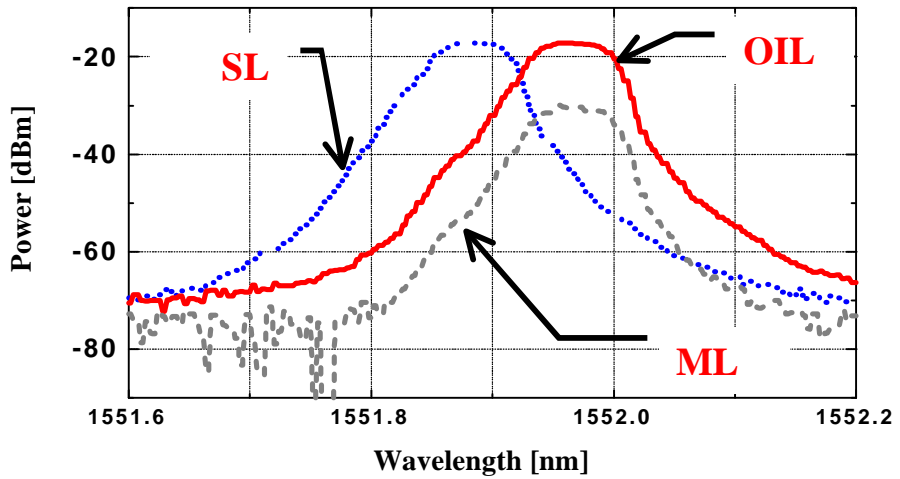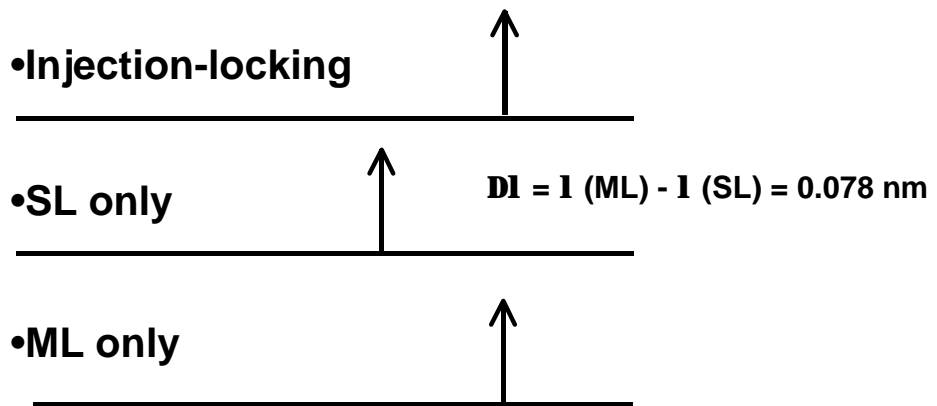
(b) Comparison of wavelength by generating OIL

Fig. 3-1. Optical spectra and comparison of wavelength by OIL

3.2 Characteristics of Injection Locking Method

3.2.1. Non-linearity Improvement

The optical analog transmission of GHz range signals is recently attracting much interest for WLL (Wireless Local Loop), CATV, and satellite system applications. In these applications, direct modulation of a semiconductor laser diode is used for transmitting signals multiplexed by RF range subcarriers. Consequently, the LD (Laser Diode) non-linearity becomes a key issue in the system performance because it can interfere and limit the number of channels as well as transmission distance [44].

One method of overcoming the LD non-linearity problem is using the optical injection locking (OIL) technique, where light from an external laser (Master laser) is injected into the signal transmitting laser (Slaver laser) as shown in Fig. 4-1. When slave laser is locked to master laser, it can have modulation bandwidth enhancement and chirp/noise reduction [45]. We perform numerical analysis of injection locked lasers to show that injection locking improves LD non-linearity characteristics. The numerical analysis of injection locked lasers is based on Lang's equations in which the laser non-linearity characteristics are described with the gain suppression term in the rate equations. The simulation parameters are obtained from reference [39]. For the simulation, two RF-sources (f_1 = 2.5 GHz and f_2 = 2.7 GHz) with the same amplitude are used in order to directly modulate the slave laser. The slave laser

output spectrum is obtained by fast-Fourier-transforming the output power of slave laser calculated by the Runge-Kutta integration of Lang's equations.

Figure 3-2 shows the amplitudes for fundamental and harmonic components of LD output spectra as function of amplitude for (a) free-running and (b) injection locked lasers. The second inter-modulation products (IMPs) at $f_1 + f_2$ and $2f_1$, and third IMP at $2f_2 - f_1$ are smaller for injection locked LD than for free-running LD. The slight difference in the amplitude of the fundamental term (f_1) is due to the change in LD dynamic characteristics caused by injection locking. Amplitudes of several frequency components are compared for free-running and OIL cases in Fig. 3-2.
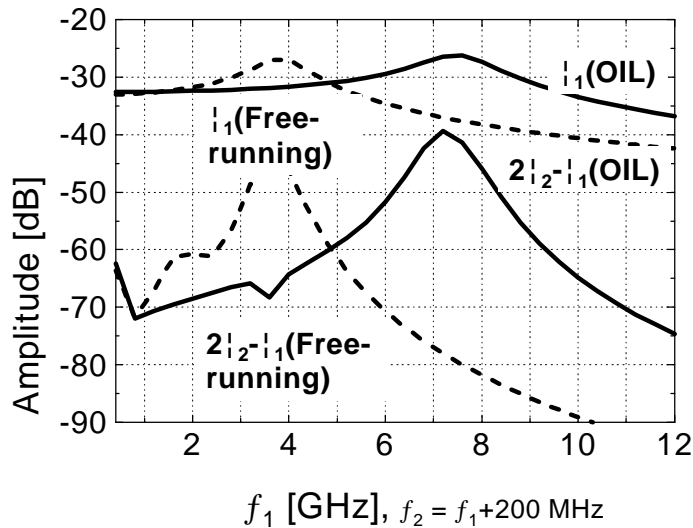
Fig. 3-2. Simulated modulation frequency responses at f_1 and $2f_2 - f_1$ for free-running and injection-locked lasers

3.2.2 Direct Modulation Bandwidth Enhancement

There are renewed research efforts for injection-locked laser diodes as they can provide enhanced performance for various applications [49, 50]. The single mode rate equations for injection locked lasers are employed as follows [46-48].

$$\frac{dS}{dt} = (G - g)S + \frac{1}{L}u_g S\sqrt{\frac{S_i}{S}}\cos q + R \tag{3-1}$$

$$\frac{d\Phi}{dt} = (w_j - w_o) + \frac{1}{2L}u_g\sqrt{\frac{S_i}{S}}\sin q \tag{3-2}$$

$$\frac{dN}{dt} = -\frac{N}{t_e} - GS + \frac{I}{q} \tag{3-3}$$

where, S_i is the photon number injected into SL from ML through the optical isolator between them, and S is the photon number in the cavity of SL. By the small signal analysis of these equations, the third order system function for injection-locked frequency response can be obtained. For free running laser diodes, the frequency response system function is of the second order.

We first found the maximally allowed phase detuning range between ML and SL. In order to be stable for the system, its poles should be located in the left plane in s-domain. Figure 3-3 shows the allowed phase detuning range for a fixed injection levels. The maximally allowed phase detuning value becomes larger as the injected photon number gets increased.

Figure 3-4 shows the direct modulation response for several injection

levels at the allowed maximum phase detuning values. It shows clearly that a stronger injection locking can provide larger direct modulation bandwidth. For example, the modulation bandwidth of an injection-locked laser at (S_i/S) = -5 dB is about three times larger than that of a free-running laser.

Figure 3-3 shows modulation response for several phase detuning values with injection level fixed at –5 dB. Larger modulation bandwidth can be achieved by detuning the ML's phase. The resonance frequency of the injection-locked laser can be obtained for several injection-levels within each allowed frequency detuning range. The frequency detuning, $Dw = w_{ML} - w_{SL}$, can be determined from the following equation.

$$\Delta w = w_{ML} - w_{SL}$$
$$= \frac{1}{2} a \left[\Gamma n_g a_o (N - n_t) - \frac{1}{t_p} \right] + K_c \sqrt{\frac{P_{in}}{P}} \sin q \qquad (3\text{-}4)$$

Here, α is the linewidth enhancement factor. The modulation response is a strong function of applied injection level and phase/frequency detuning values.
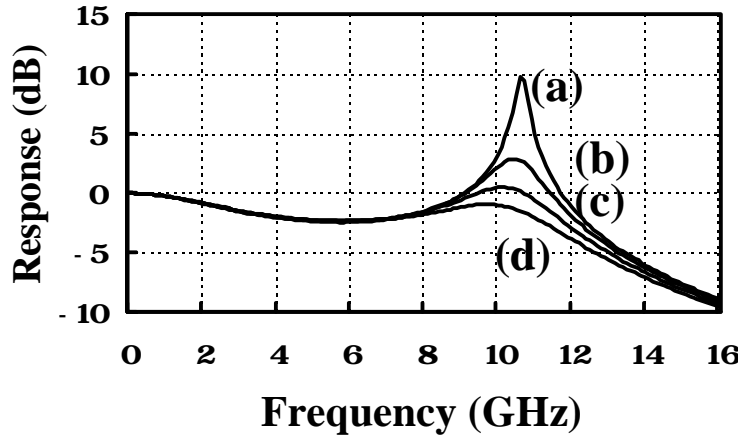
Fig. 3-3. Modulation response at a fixed injection level of –5 dB over phase

detuning values, such as (a) 83 deg., (b) 80 deg., (c) 70 deg., and (d)

60 deg.
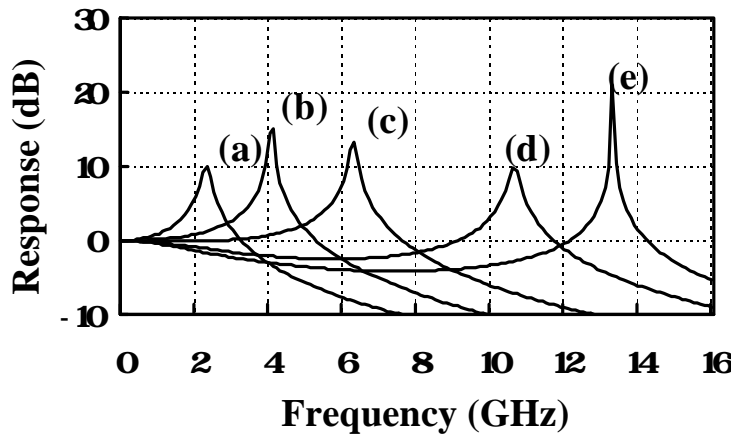
Fig. 3-4. Modulation response for several injection levels with allowed phase

detuning values, such as (a) free running laser, (b) (S_i/S) = -15 dB (q =

48 deg.), (c) (S_i/S) = -10 dB (q = 71 deg.), (d) (S_i/S) = -5 dB (q = 83

deg.), and (e) (S_i/S) = -3 dB (q = 85 deg.)

Chapter 4. Simulation Results

4.1 Optical Injection Locking Configuration

The optical injection locking configuration is made up of ML and SL as shown in Fig. 4-1, where the CW ML light is injected into the SL cavity. Two lasers have a frequency offset of Δf, where Δf is defined as f_{ML} - f_{SL}. It is assumed that the injected ML light has the same polarization as SL by the proper control of the polarization controller located between the two lasers.

4.2 Analysis of Spectral Characteristics of Semiconductor Lasers under Optical Injection

4.2.1 Single Mode OIL Rate Equation

Assuming DFB lasers with negligible sidemodes are used for both ML and SL, the SL under the influence of external light injection can be described by the following single mode rate equations shown below [51].

$$\frac{dP}{dt} = \left[\frac{\Gamma g_0}{1+eP}(N-n_t) - \frac{1}{t_p}\right]P + \frac{\Gamma b}{t_n}N + 2K_C\sqrt{P_{in}P}\cos(\Phi_{ML}-\Phi) \tag{4-1}$$

$$\frac{d\Phi}{dt} = -2p\Delta f + \frac{1}{2}a\left[\Gamma g_0(N-n_t) - \frac{1}{t_p}\right] + K_C\sqrt{\frac{P_{in}}{P}}\sin(\Phi_{ML}-\Phi) \tag{4-2}$$

$$\frac{dN}{dt} = \frac{I}{qV_a} - \frac{g_0}{1+eP}(N-n_t)P - \frac{N}{t_n} \tag{4-3}$$

In the above equations, P_{in} and Φ_{ML} represent the density and the phase of the injected photons and K_C ($= \boldsymbol{u}_g/2L_a$) is the coupling rate between ML and SL.

Other parameters have the usual meanings. The numerical values for the laser parameters used are obtained from reference [66].

Table 2. Parameter values in the numerical simulations

Symbol	Parameter	Value	Unit
	lasing wavelength	1550	nm
	confinement factor	0.4	
n_t	transparent carrier density	1.0×10^{18}	cm^{-3}
p	photon lifetime	3.0×10^{-12}	sec
n	carrier lifetime	1.0×10^{-9}	sec
	spontaneous emission factor	3.0×10^{-5}	
g	group velocity	8.5×10^{9}	cm/sec
g_0	differential gain	12.7×10^{-7}	cm^3/sec
	gain suppression factor	5.0×10^{-17}	cm^3
V_a	volume of active layer	1.5×10^{-10}	cm^3
	linewidth enhancement factor	5	
ex	LD differential quantum efficiency	0.4	
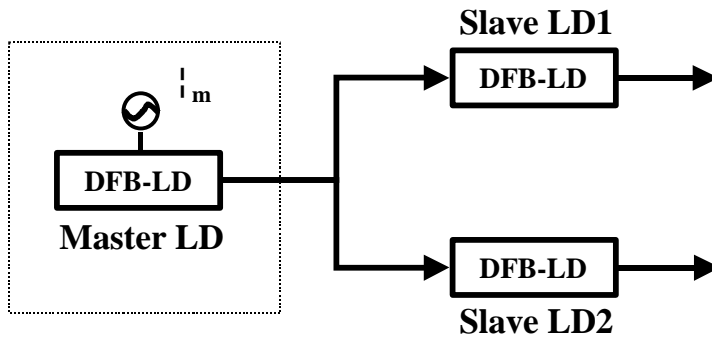
(a)
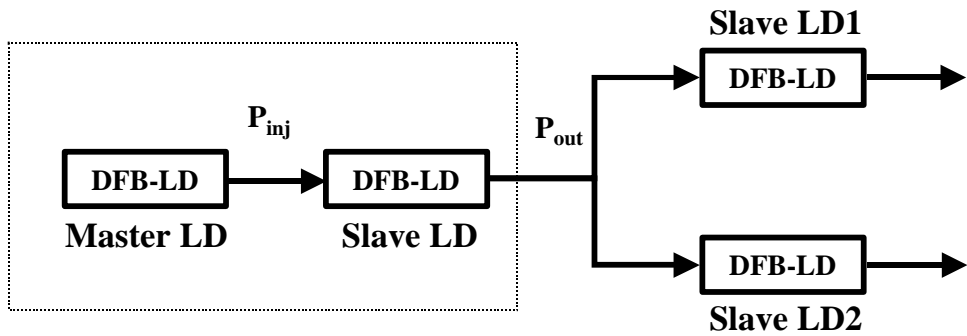
(b)

Fig. 4-1. Block diagram for (a) the typical and (b) the proposed OIL

technique for μ/mm-wave generation

4.2.2 Injection Locking Property

From the steady-state analysis of the rate equations, Fig. 4-2 shows the locking and unlocking regions as function of Δf and R. Here, injection power ratio R is defined as P_{inj}/P_{out}, where P_{inj} is the injected optical power just outside the SL facet and P_{out} is SL output power. For the results shown in Fig. 4-2, SL output power is fixed at 2 mW. If the gain suppression and the spontaneous emission terms are ignored, the range of Δf that allows locking can be determined as follows [52].

$$\left| \Delta f (= f_{ML} - f_{SL}) \right| \leq \frac{K_C}{2\boldsymbol{p}} \sqrt{\frac{P_{in}}{P}(1+\boldsymbol{a}^2)} \qquad (4\text{-}4)$$

This locking range can be further classified into two distinctive regimes : stable-locking and unstable locking. In the stable locking regime, the output power converges to a steady-state value when a small perturbation is introduced. In the unstable locking regime, however, the power does not converge to the steady-state value but experiences a self-sustained oscillation or even chaos when a small perturbation is introduced. Such an oscillation and chaos produce multiple sidebands in the output optical spectra. The range for the stable-locking regime can be determined by the s-domain stability analysis of the linearized rate equations above. The shaded area inside the unstable locking regime in Fig. 4-2 represents the place where the chaos occurs. The

chaos area outside the locking regimes is not taken into account here. The asymmetry of the stable-locking regime is dependent on R. The center of the stable-locking bandwidth is shifted toward the shorter frequency from the SL lasing frequency with increasing R.
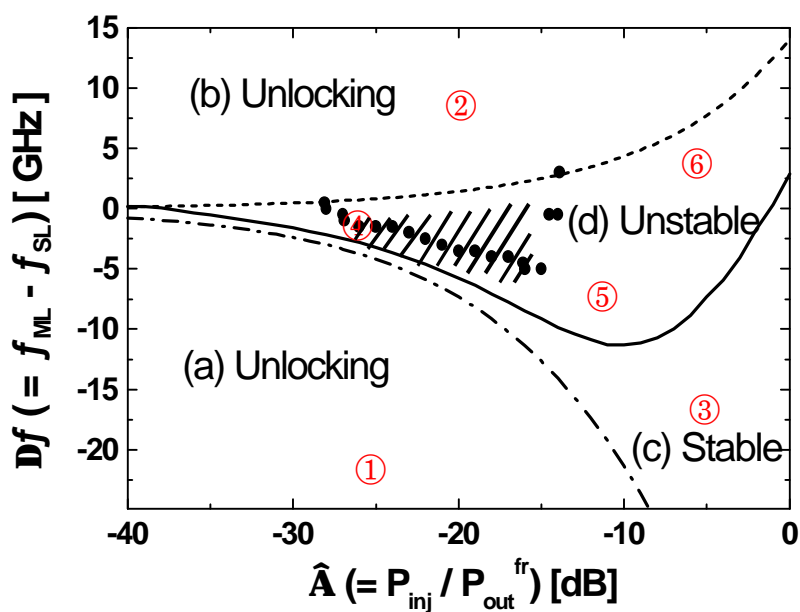
Fig. 4-2. Locking range versus injection power ratio

4.2.3 Transient Analysis

This dissertation deals with the characteristics of injection locking for semiconductor lasers by large signal and spectra analysis. Figure 4-1 shows a basic injection-locking configuration. Optical power from Master laser goes through isolator and is injected to slave laser. We use a laser diode parameters in reference [39] and single mode Van der Pol equation to model numerical injetion-locking method [9]. Boundary condition of locking region in steady state is as follows [11].

$$
\begin{aligned}
\Delta \boldsymbol{w} &= 2\boldsymbol{p}(f_{ML} - f_{SL}) \\
&= K_c \sqrt{\frac{S_{ML}}{S_{SL}}}(\sin \boldsymbol{q} - \boldsymbol{a}\cos \boldsymbol{q})
\end{aligned} \tag{4-5}
$$

K_c is coupling coefficient, S_{ML} is photon density injected from ML (Master Laser) to SL (Slave Laser), S_{SL} is photon density in SL cavity, and $\boldsymbol{q}$ is a phase difference between ML and SL. By analyzing small signal analysis in given rate equation, all zeros are located in left s-domain to lock statically stable in 3 rd order system function. We have been showed values to satisfy stability analysis in Fig. 4-2. From the figures, it is divided into stable-locking, unstable locking and unlocked region. We can expect signal response and spectrum given values in Fig. 4-2. In the case of signal response, waveform is depicted under injected step-like current from $1.01 I_{th}$ to $1.5 I_{th}$ at 2ns.

Waveforms by FFT transformation after deriving portion of steady state at the window after overshoot transient response are shown in Fig. 4-3. Each value is normalized by high values obtained from FFT outputs in the case of free-running state. We can estimate all optical power of SL locked in ML frequency in stable locking. The theoretical power spectra were calculated by taking the fast Fourier Transform (FFT) of the steady-state slave intracavity electric field over a given time window. In the case of unstable locking, we can define locked state in a wide expression but power in locked state is vibrating in the center of steady state and it is not stable locked as shown in Fig. 4-4(c) because unlocked power is not in this state. Spectrum of sideband in Fig. 4-4(c) stems from relaxation oscillation sideband. In the case of unlocked state, power reaches in constant steady state as unlocked power is increased contrary to the reduction of power of ML frequency in locked state.
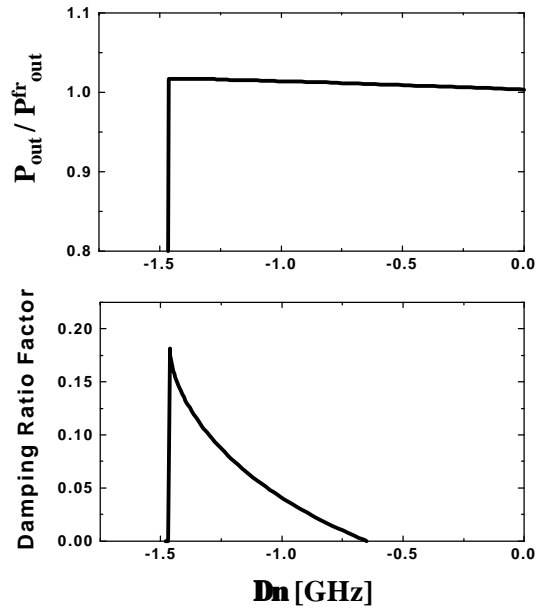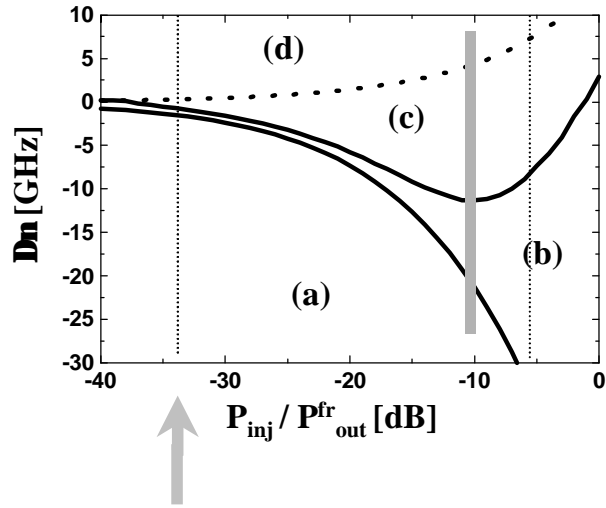
(a) Weak optical injection
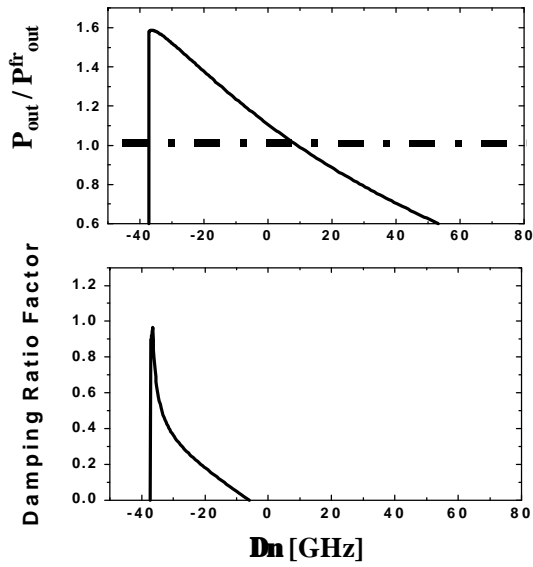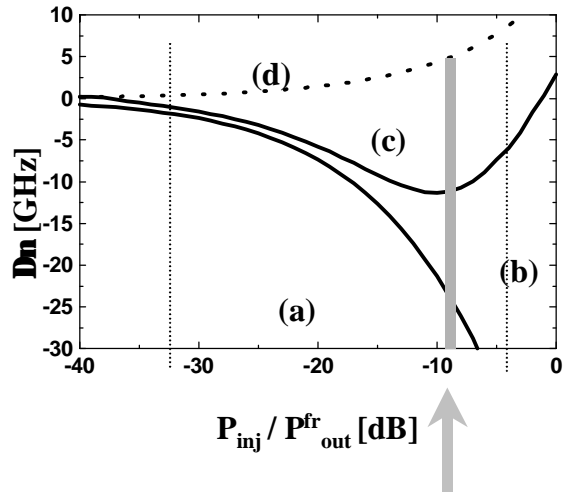
(b) Strong optical injection

Fig. 4-3. Locking characteristics of weak and strong optical injection
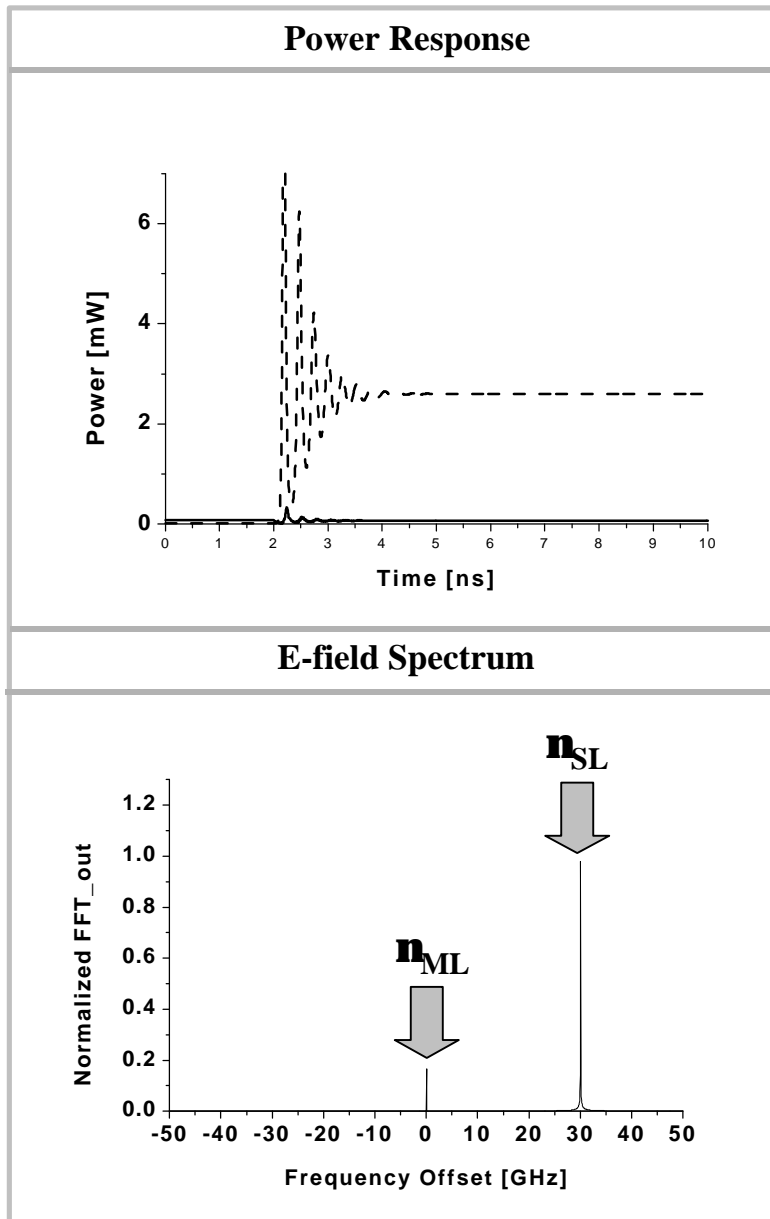
Power Response

E-field Spectrum

(a) Unlocked(Lower)
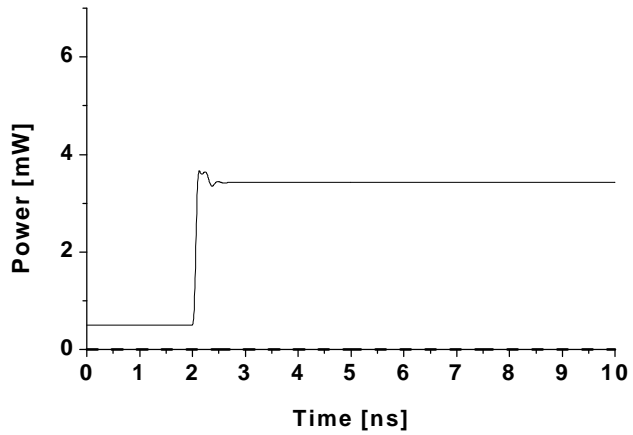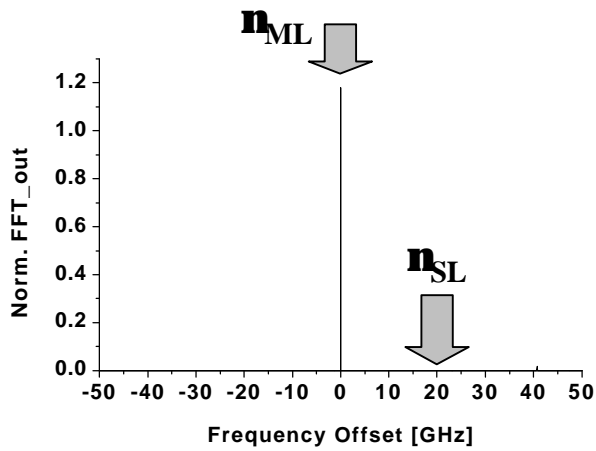
(b) Stable

Power Response
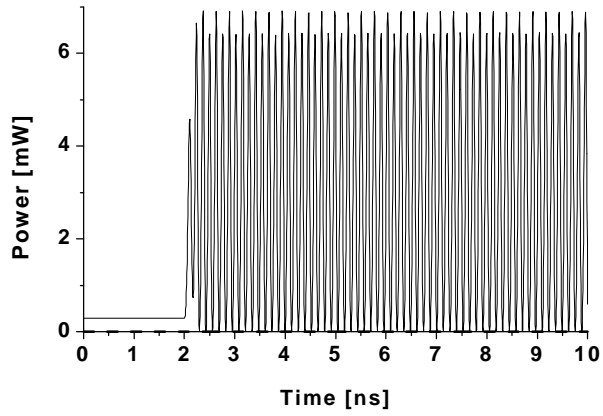
E-field Spectrum

(c) Unstable

Power Response
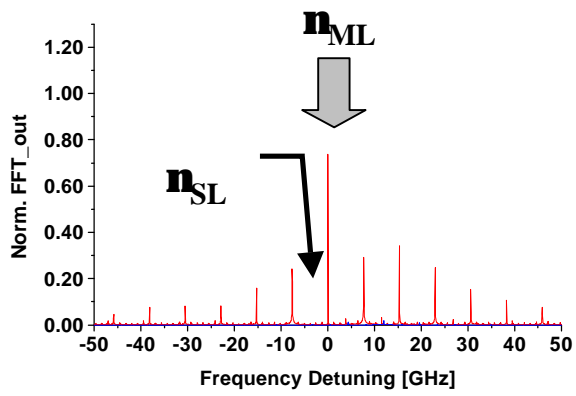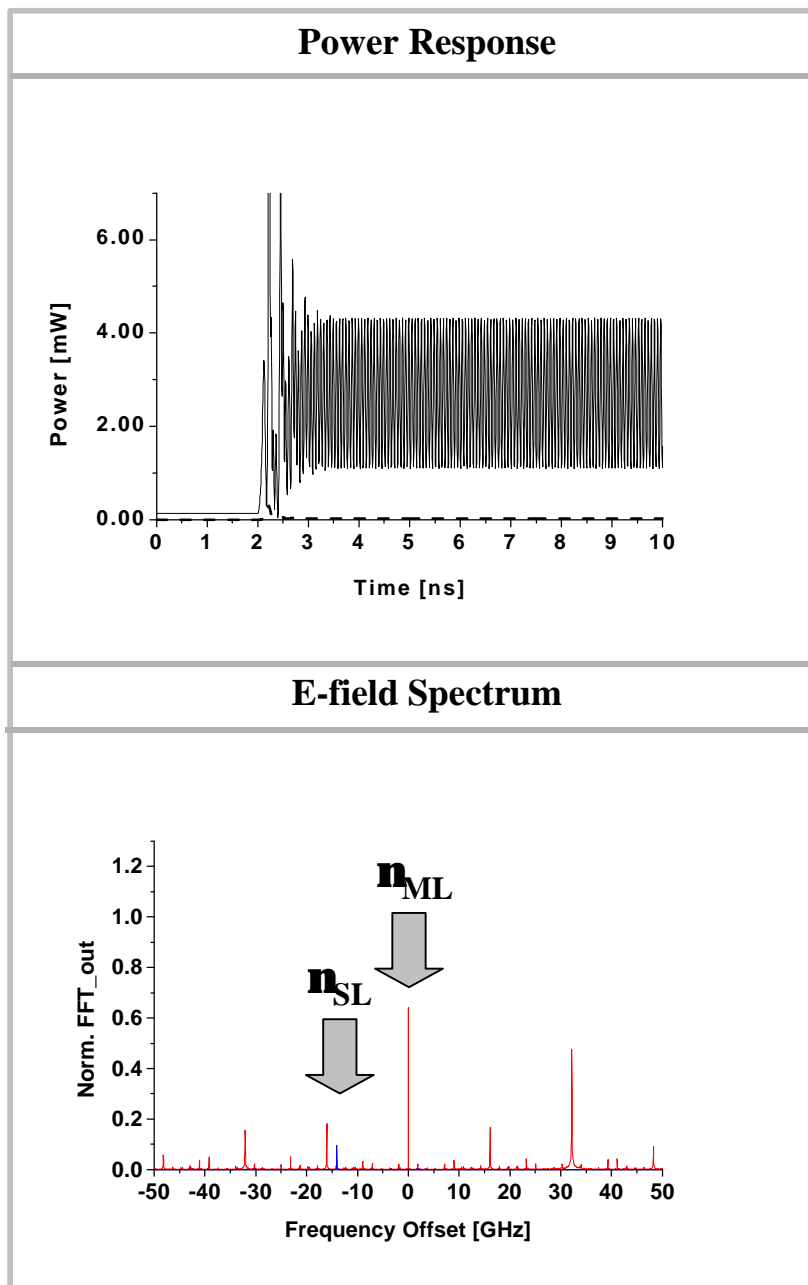
E-field Spectrum

(d) Unstable (Upper)

Fig. 4-4. Power response and E field spectrum in locking condition

4.2.4 Transient Response and Spectrum for Locking Regime

One method of generating optical μ/mm-wave signals is to use the optical injection locking (OIL) technique [54]. In this technique, the master laser (ML) is directly RF-modulated and has multiple optical sidebands which separated by the modulation frequency, f_m. Two slave lasers (SL's) are then injection-locked by two sidebands separated by the desired frequency offset, generating two coherent optical signals can produce the desired beat frequency signal in the photodetector. In order to obtain high frequency signals, the *rf*-modulated ML should provide a large number of sidebands that are widely separated. The sideband generation, however, sensitively depends on the modulating RF-power and frequency. A technique that does not require external RF source would be highly desirable. Realizing such an OIL system is the goal of the present investigation.

Recent studies on OIL have found that the modulation bandwidth of a semiconductor laser can be significantly enhanced under the strong optical injection. However, the locking properties under the strong optical injection have not been fully analyzed outside the dynamically stable locking range, where such effects as undamped relaxation oscillation and chaos can occur. We analyze the spectral characteristics of semiconductor lasers under strong optical injection, and show that the generation of multiple optical sidebands having large frequency separation is possible. By feeding these sidebands into two SL's, as shown in Fig. 4-12, it is possible to generate optical μ/mm-waves

without using any external RF source. When light from ML is injected into SL, the locking characteristics can be classified into three distinctive regimes : unlocking, dynamically stable locking, and dynamically unstable locking. Both dynamically stable and unstable locking regimes can be grouped together as the static locking regime. These characteristics are determined based on the injected optical power and the lasing frequency offset between ML and SL. For the analysis, the laser rate-equations including injected light [56, 57] are used for a sample LD whose parameters are obtained from [39]. Figure 4-2 maps the characteristic regimes determined from the rate-equation analysis. In the figure, Δf is the frequency difference between the ML (f_{ML}) and SL lasing frequency (f_{SL}), and the injection power ratio, $\Re$, is the ratio between the injected ML optical power (P_{inj}) and SL optical power (P_{out}^{fr}) without optical injection. The boundaries for the static locking regime can be obtained from the steady-state solutions of the OIL rate equations. Within the static locking regime, the stability analysis of the linearized transfer function determines the dynamically stable locking regime. The calculated power spectra at the operating points ①~⑥ in Fig. 4-2 are illustrated in Fig. 4-5. These are obtained by Fourier transforming the SL output power at the steady-state determined from the large-signal numerical analysis of the rate-equations. The calculated spectra are normalized with the SL's spectral peak value under no optical injection. In the calculations, noises are neglected and SL is biased at $1.5I_{th}$. The zero for the horizontal axis is f_{ML}. The power spectrum for Fig. 4-2(①) is typical for the unlocking regime. Unlocked power exists only at f_{SL}. On the

other hand, the power spectrum for another unlocking region at Fig.4-2(②) having positive Δf. Here, the injected light is amplified and beats the SL light. This causes the four wave mixing between ML and SL light and generates multiple conjugate sidemodes. The sidemode separation, $\Delta\nu$, equals Δf but this region is not useful for optical μ/mm-wave signal generation since the conjugate sidemodes are not coherent. Figure 4-2(③) shows the power spectrum at the dynamically stable regime. Here, SL is locked to ML and has power spectrum only at f_{ML}. The dynamically unstable locking regime is characterized by undamped relaxation oscillation and chaos. Figure 4-4(③) shows the case of chaos, where the spectrum is densely spreaded. We find that chaos occurs when $\Re$ is less than about -14 dB, as indicated by shades in the figure. This agrees with the experimental and analytical results [12]. When $\Re$ > -14 dB, the undamped relaxation sidebands appear and their separation becomes larger for increasing $\Re$ and Δf. The maximum possible $\Delta\nu$ as function of $\Re$ is illustrated in Fig. 4-10. When two SL's are locked to two of the sidebands generated in the dynamically stable regime in the manner shown in Fig. 4-5, they can act as frequency filters and suppress other undesired sidesmodes. Then, two SL's output light will be two coherent signals separated by a multiple of $\Delta\nu$ and the beat signals at the multiple of $\Delta\nu$ can be generated at the photodiode. This technique allows $\Delta\nu$ as large as 15.4 GHz at $\Re$= 0 dB in the present analysis. As an example, if two sidebands indicated by arrows in Fig. 4-9(⑤) and (⑥) are selected, the beat frequencies of 58 GHz ($\Delta\nu$ = 7.25 GHz), and 100.8 GHz ($\Delta\nu$ = 12.6 GHz) can be obtained.
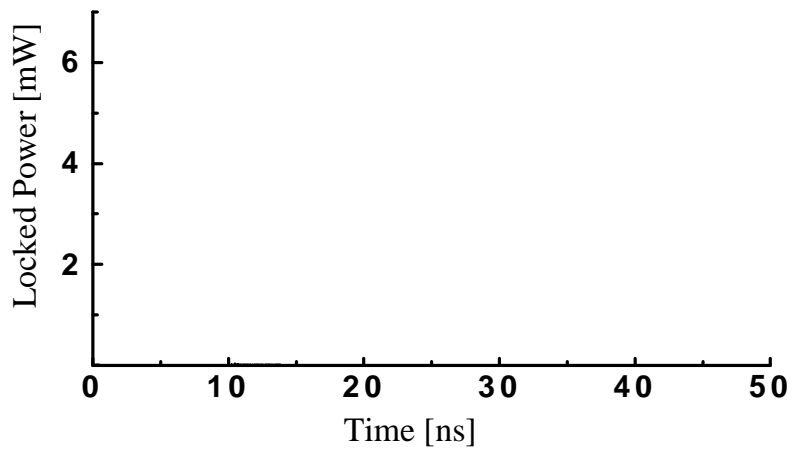
(a) Locked Power

(b)
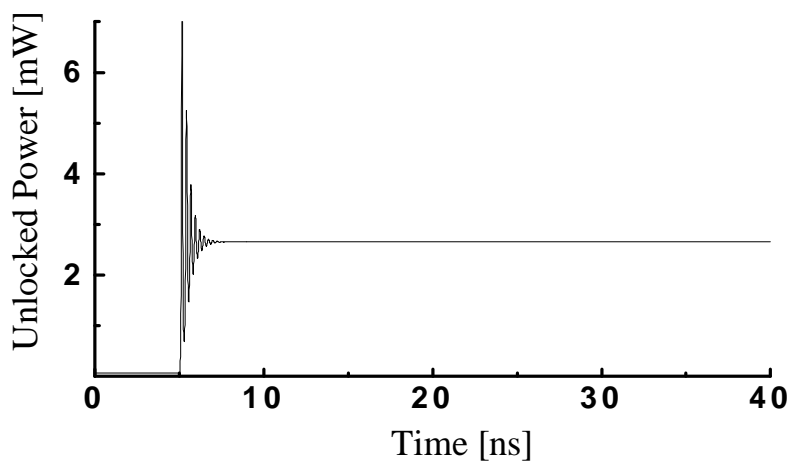
(b) Unlocked Power
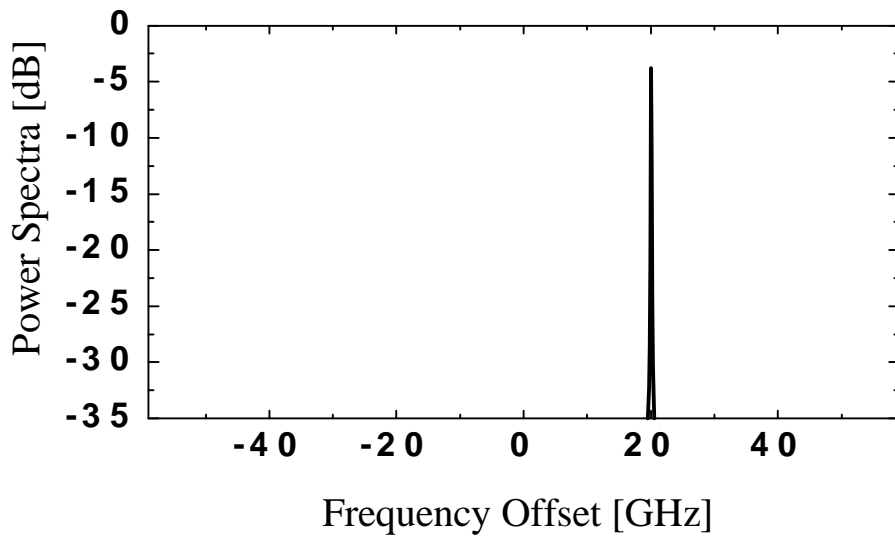
(c) Power Spectra

Fig. 4-5. Transient response and spectrum for unlocking (Lower)
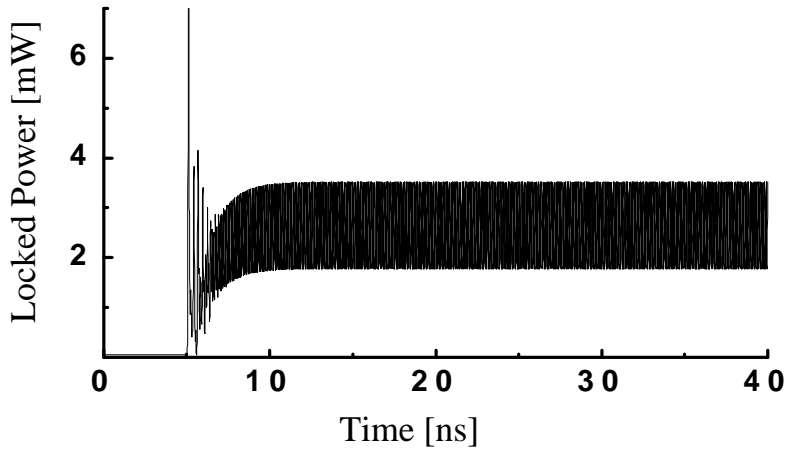
(a) Locked Power
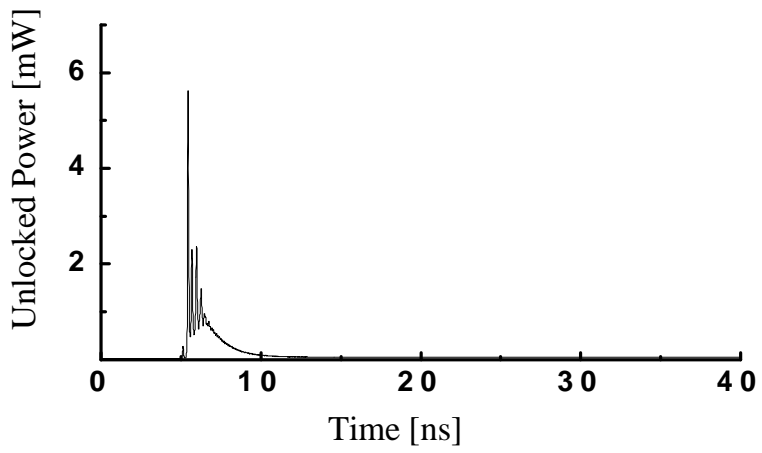
(b) Unlocked Power
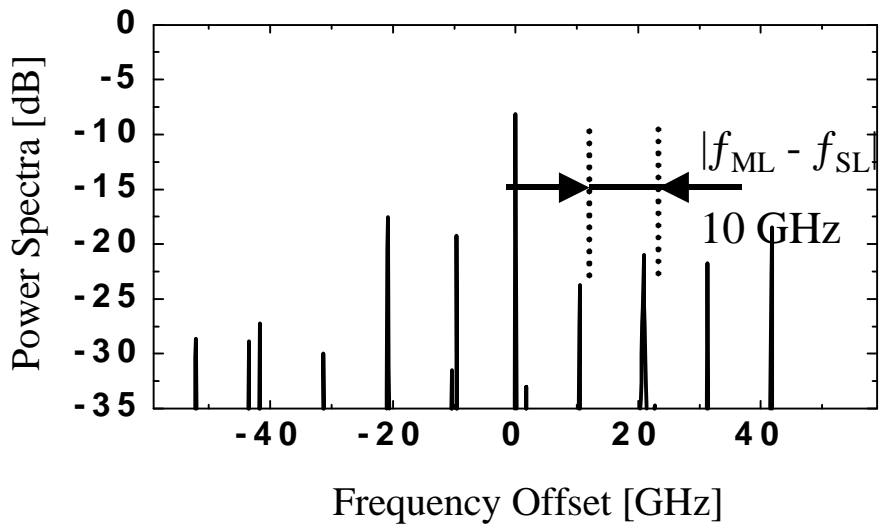
(c) Power Spectra

Fig. 4-6. Transients response and spectrum for unlocking (Upper)
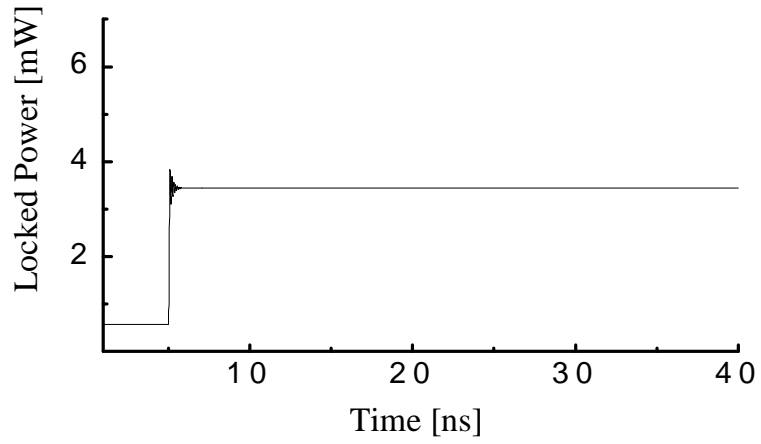
(a) Locked Power
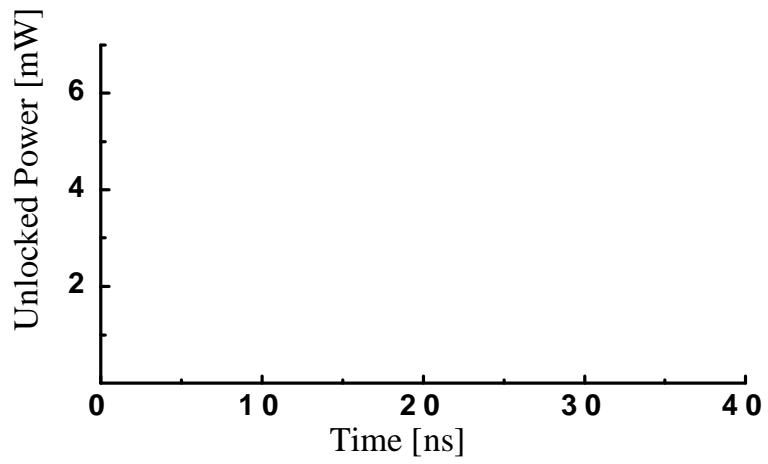
(b) Unlocked Power
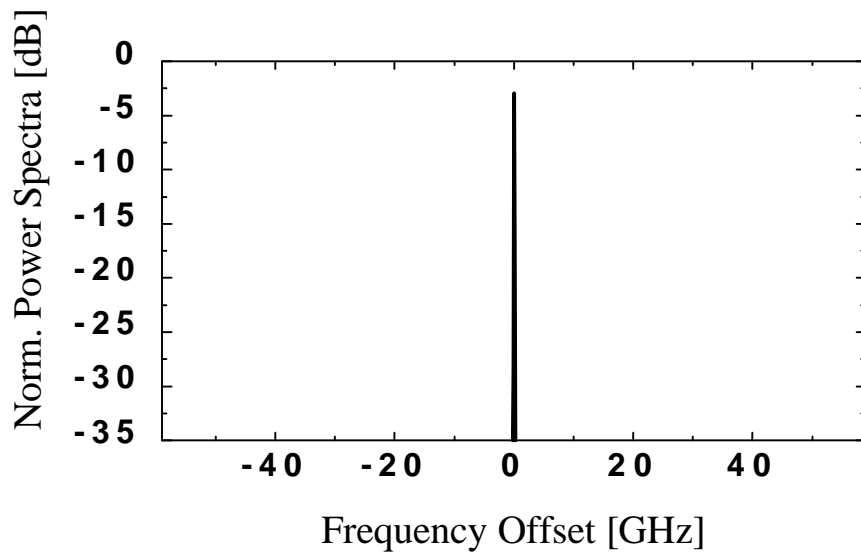
(c) Power Spectra

Fig. 4-7. Transient response and spectrum for stable locking
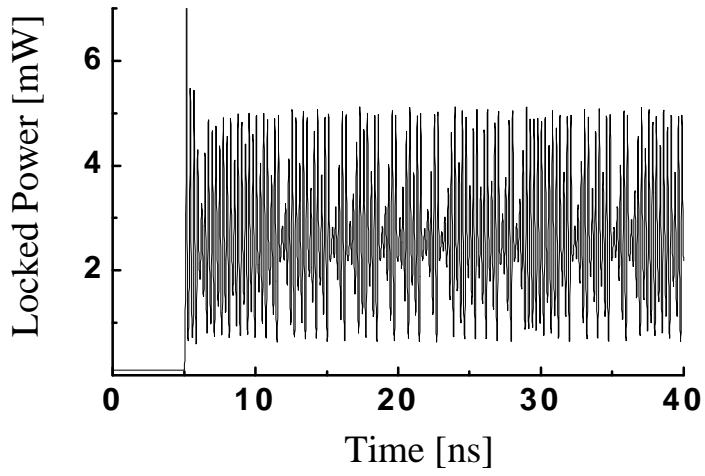
(a) Locked Power
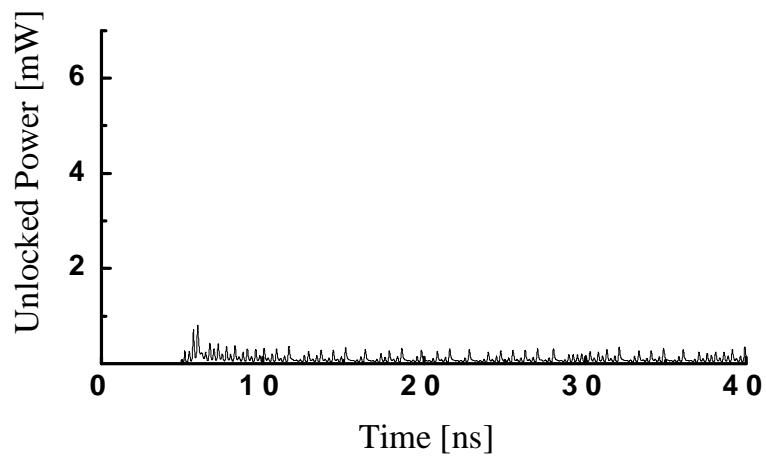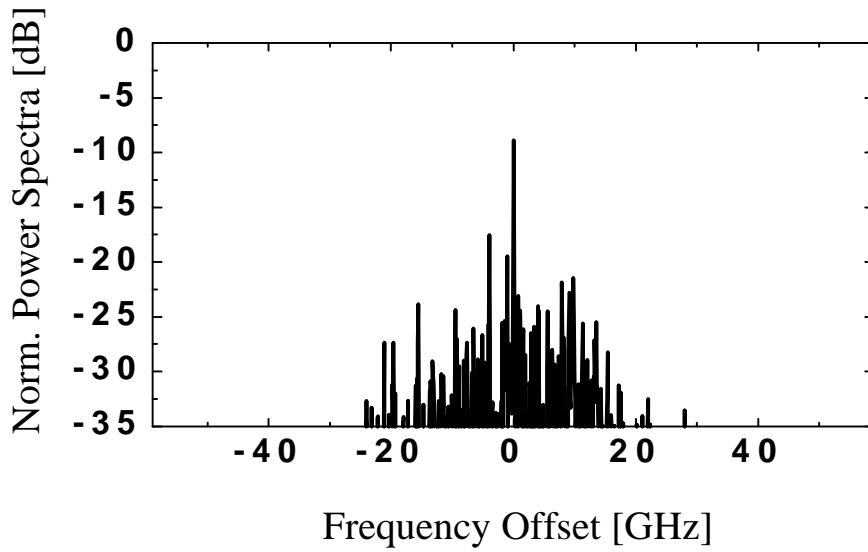
(b) Unlocked Power

(c) Power Spectra

Fig. 4-8. Transients response and spectrum for chaos
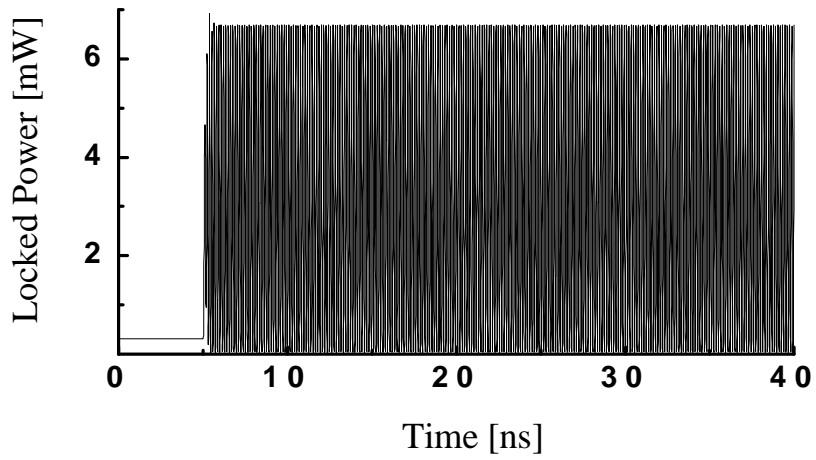
(a) Locked Power
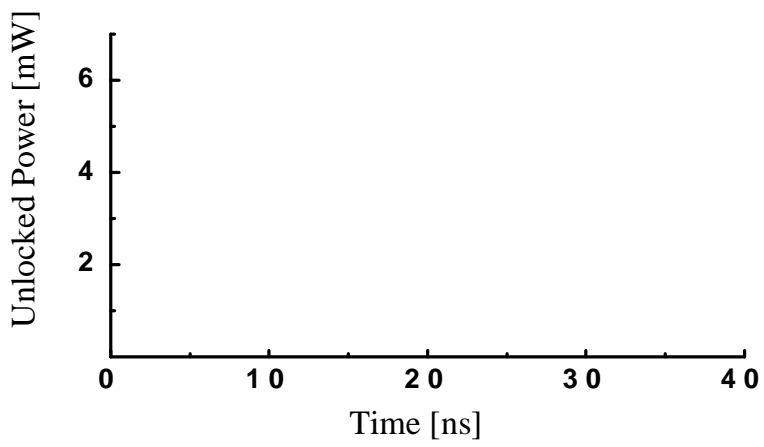
(b) Unlocked Power
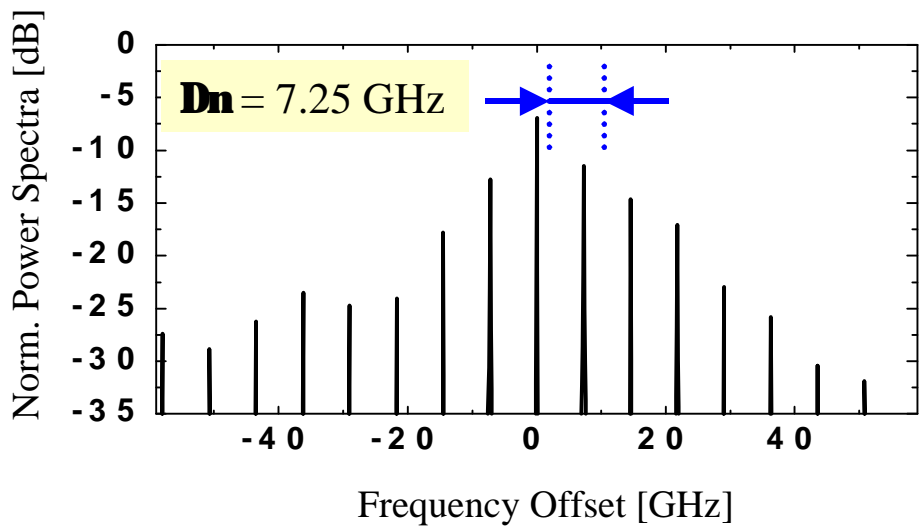
(c) Power Spectra

Fig. 4-9. Transient response and spectrum for unstable locking
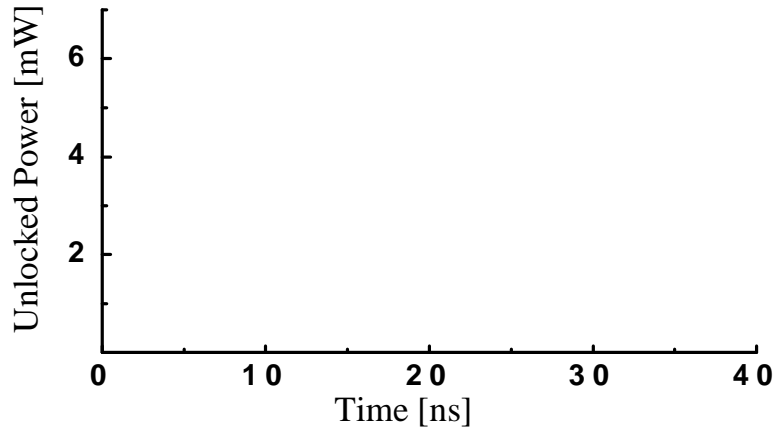
(a) Locked Power
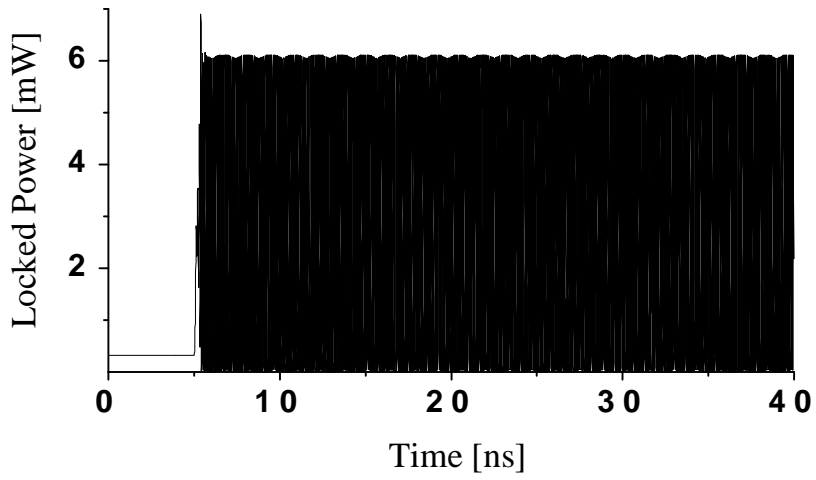
(b) Unlocked Power
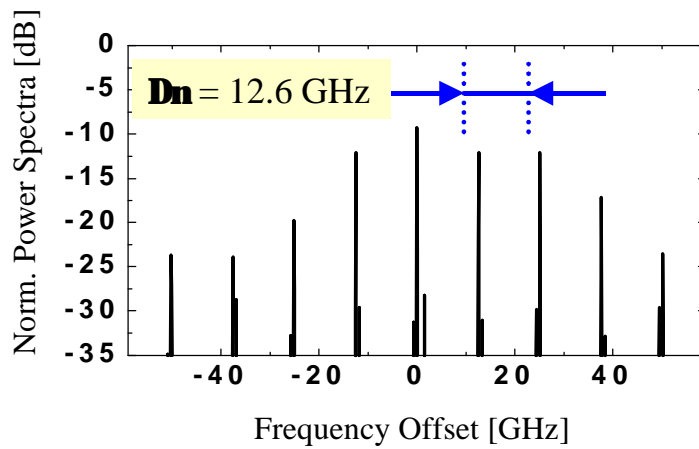
(c) Power Spectra

Fig. 4-10. Transients response and spectrum for unstable locking (different
power ratio)

4.3 Direct Modulation of Semiconductor Lasers

4.3.1 Large Signal Modulation

When the semiconductor laser is directly modulated, it is intensity modulated (IM) and frequency modulated (FM) simultaneously due to the presence of the intrinsic frequency chirp. To a first approximation, the optical output of the directly modulated semiconductor laser can be expressed by the following complex electric field [59].

$$\tilde{E} = P_0^{1/2} \left(1 + m_{IM} \cos(\Omega_m t + \Phi_{IM})\right)^{1/2} e^{j m_{FM} \sin(\Omega_m t + \Phi_{FM})} \tag{4-6}$$

P_0 is the average output power, Ω_m is the applied angular modulation frequency, m_{IM} and m_{FM} are the IM and FM indices, respectively. And, Φ_{IM} and Φ_{FM} are the corresponding phases. Eq. (4-6) shows that a directly modulated semiconductor laser has the sidebands at the harmonics of the modulation frequency in the electrical field spectrum. The electrical field in Eq. (4-6) can be expressed by a series of Bessel functions as follows [59].

$$\tilde{E} = P_0^{1/2} \sum_{k=-\infty}^{\infty} C_k e^{jk(\Omega_m t + \Phi_{IM})} \tag{4-7}$$

$$C_k = e^{jk\Delta\Phi} \left[J_k(m_{FM}) + \frac{m_{IM}}{4} \left(J_{k+1}(m_{FM}) e^{j\Delta\Phi} + J_{k-1}(m_{FM}) e^{-j\Delta\Phi} \right) \right] \tag{4-8}$$

where $\Delta\Phi$ is the phase difference between Φ_{FM} and Φ_{IM}. When the applied modulation frequency, Ω_m, is given, the modulation indices and phases in Eq. (4-6) can be analytically determined from the IM and FM responses of the linearized laser rate-equations in Eq (4-6), where no external light injection is included.

4.3.2 Dependence of the Optical Spectrum for the Different Modulation Powers

The complex electrical amplitude of each sideband of the directly modulated semiconductor laser can be denoted in Eq. (4-6). Eq. (4-6) shows the asymmetric sidebands in the optical spectrum since the IM response is superimposed on the FM response. The magnitude and quantity of the sidebands are determined directly by the FM index, m_{FM}, which has the relation with the intrinsic laser frequency chirp and increases with the modulation current as shown in Fig. 4-11. The increase of m_{FM} can make the target sideband power increase so that its power becomes larger than the center lasing peak power in the optical spectrum as illustrated in Fig. 4-11. In Fig. 4-11, it is assumed that the LD is biased at 1.5 times threshold at the modulation frequency of 3 GHz.
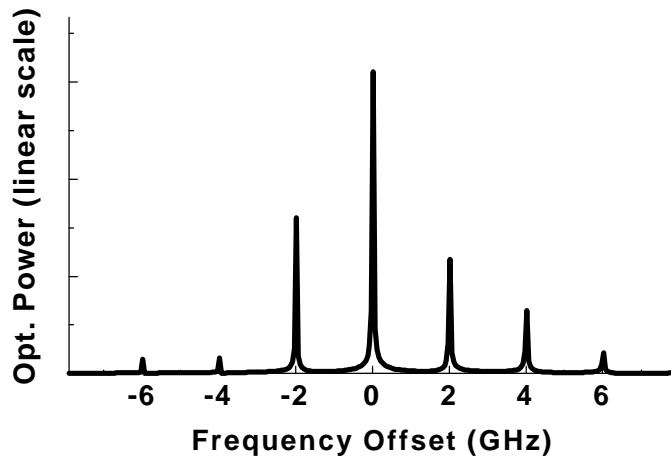
(a) $I_{mod} = 4mA$
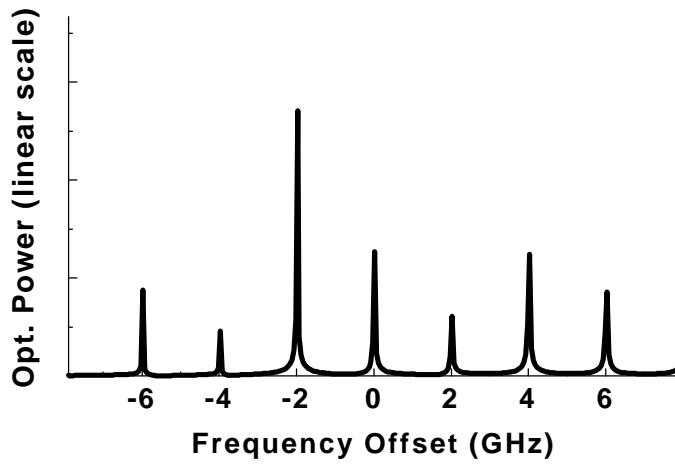
(b) $I_{mod} = 8mA$

Fig. 4-11. Dependence of the optical spectrum for the different modulation
Powers

4.3.3. Modeling of Slave Lasers Locked to the Sidebands of the Master Laser

If two target sidebands with the desired frequency separation are selected among the multiple ML sidebands and beat each other in PD, the desired beat signal can be obtained in the RF spectrum. Figure 4-12 shows the block diagram for the sideband selection using optical injection locking method, where two SLs are locked to the target sidebands generated from the directly modulated ML. The rate-equations in Eq. (4-1~3) represent the semiconductor lasers under the CW master light, but are not appropriate in expressing the semiconductor lasers in the presence of the multiple ML sidebands. In order to investigate the effect of the presence of the multiple ML sidebands on the SL spectral characteristics, we have adopted the Lang's equations based on the complex electrical field [39]. Then, we have extended those equations representing the LD under the multiple lights as follows.

$$\frac{dE_k}{dt} = \frac{1}{2}\left(\Gamma G(N) - \frac{1}{t_p}\right)\cdot(1-j\boldsymbol{a})\cdot E_k + j\left(\boldsymbol{w}_k^{ML} - \boldsymbol{w}^{fr}\right)\cdot E_k + 2K_C E_k^{ML} \tag{4-9}$$

$$\frac{dP_u}{dt} = \left(\Gamma G(N) - \frac{1}{t_p}\right)\cdot P_u + \Gamma\boldsymbol{b}\frac{N}{t_n} \tag{4-10}$$

$$\frac{dN}{dt} = \frac{I}{qV_a} - G(N)\cdot\left(P_u + \sum_k|E_k|^2\right) - \frac{N}{t_n} \tag{4-11}$$

$$G(N) = \frac{g_0(N-n_t)}{1+\boldsymbol{e}\left(P_u + \sum_k|E_k|^2\right)} \tag{4-12}$$

In the above equations, E_k represents the normalized complex electrical field

that is locked to the k-th ML sideband whose normalized complex electrical field and angular frequency are denoted by $E_k{}^{ML}$ and $\boldsymbol{w}_k{}^{ML}$, respectively. $|E_k|^2$ corresponds to the locked normalized photon density for the k-th ML sideband $\boldsymbol{w}^{fr}$ is the lasing angular frequency for the free-running SL (no light injection). P_u is the unlocked normalized photon density. The Langevin noise terms are not expected to influence our investigation and, consequently, not included in the above equations. The coupling rate (K_C) is defined as $\boldsymbol{u}_g/2L$. The value of 141.7 GHz is used for K_C in our investigation, which corresponds to the SL cavity length (L) of 300 μm.. Other parameters have the usual meanings [61]. These extended rate-equations can include the arbitrary number of the ML sidebands, whereas Lang's model [7] deals with the SL under the single mode laser injection, that is, only one value for k is considered in the above equations. The field amplitude of the k-th ML sideband ($E_k{}^{ML}$) is determined from m_{FM} which is directly related to the intrinsic laser frequency chirp characteristics. The ML field at the fundamental lasing frequency is denoted by $E_0{}^{ML}$. The negative (positive) sign for k means that the sideband is located at the smaller (larger) frequency than the fundamental frequency ($k = 0$). The angular frequency of the k-th ML sideband ($\boldsymbol{w}_k{}^{ML}$) can be simply expressed as $\boldsymbol{w}_k{}^{ML} = \boldsymbol{w}_0{}^{ML} + k \times \Omega_m$.

For the numerical simulation, it is assumed that three identical semiconductor lasers are used for one ML and two SLs. It is also assumed that the ML is biased at $1.57 \times I_{th}$ (the calculated threshold current, $I_{th,}$ from the parameters used is 33.5 mA) and is RF- modulated at 8 GHz with the

modulation current I_m of 25 mA. m_{IM} and m_{FM} can be calculated for the given conditions using linearized laser rate-equations, and the values of 0.4 and 2.7 are obtained for m_{IM} and m_{FM}, respectively. With these, the ML optical spectrum has ±2 ML sideband larger than other sidebands. The total of 17 ML sidebands including the fundamental peak are considered for our analysis. We designated   +2 and -2 sidebands as target sidebands for injection-locking two SLs so that 32 GHz beat signal can be generated. Under these conditions, the effects of the unselected sidebands on the spectral characteristics of the beat signal are investigated at different ML injection powers. We have not considered the path length differences between ML and two SLs, and between SLs to PD, which can cause the relative optical phase deviation and degrade the overall system performance [4]. The PD is simply assumed an ideal square law device for the incident optical field.

The outputs of two SLs, which are locked to the ML target sidebands, are independently solved by the fourth-order Runge-Kutta integration of Eq. (4-9~12).   Both SLs are assumed biased at $1.96 \times I_{th}$, emitting the optical power of around 5 mW when there is no ML light injection. The rate-equations are integrated over 10000 iterations with a time step of 2-ps. After the steady state is reached in the SL output light, the SL optical spectra are obtained by Fourier-transformation of the SL optical spectra. The resulting two SL spectra are summed in the optical spectrum with the frequency difference between two SLs taken into account. The optical field in the time domain is obtained from the inverse Fourier-transformation of this and the photo-detected currents are

obtained by squaring the resulting optical field. Finally, the RF spectrum of the beat signals can be calculated by the Fourier-transformation of the photo-detected currents. The frequency locking range within which SL is locked to the k-th ML sideband can be simply given as [12].

$$\left| \Delta f_k \right| \le \frac{K_C}{2\boldsymbol{p}} \sqrt{\frac{\left| E_k^{ML} \right|^2}{S}(1+\boldsymbol{a}^2)} \; . \tag{4-13}$$

This locking range can be further classified into two distinctive regimes : stable locking and unstable locking. In the stable locking regime, the output power converges to a steady-state value when a small perturbation is introduced. In the unstable locking regime, however, the power does not converge to the steady-state value but experiences a self-sustained oscillation or even chaos when a small perturbation is introduced. When the single mode ML light is assumed, the stable locking range can be determined from the s-domain stability analysis of the linearized Lang's rate-equations. However, in our case, this method can not be used, as there is more than one mode of ML light injected. In order to consider the influence of the several sidebands on the stable locking range, we determine the stable locking range in the following manner. We first numerically solve the rate-equations of Eq. (4-9~12) with the SL frequency detuned (Δf_k) in steps of 100 MHz from the k-th target sideband, where $\Delta f_k = \left(\boldsymbol{w}_k^{ML} - \boldsymbol{w}_k^{SL} \right)/2\boldsymbol{p}$. From the obtained solutions in the time domain, we judge whether or not the SLs are locked to the k-th target sidebands using

the following criteria. First, the locked photon density for the k-th target sideband should be larger than the unlocked photon density, that is, $|E_k|^2 > S_u$ ($k = \pm 2$). Second, the locked photon density for the k-th target sideband should be larger than any other locked photon densities for other sidebands, that is, $|E_k|^2 > |P_U|^2$ ($m \neq \pm 2$). Note here that it is possible to have more than one sideband within a particular locking-range. Finally, the relaxation oscillation of the locked photon density should be sufficiently suppressed after reaching the steady state. We use the suppression ratio of 30 dB for our investigation, where

$$\text{suppression ratio} \equiv \frac{\max(|E_k(t)|^2) - \min(|E_k(t)|^2)}{\max(|E_k(t)|^2) + \min(|E_k(t)|^2)} \tag{4-14}$$

With these, we are able to determine the stable locking range for the SLs locked to +2 and –2 sidebands at different injection ratios, R, which is defined as the ratio between the average ML injection power and the free-running SL power. The calculated results are shown in Fig. 4-13. It is found that the center of the stable locking range is shifted toward lower frequency from the SL lasing frequency as the injection ratio increases. Similar dependence of the stable locking range on the injection ratio has been shown from the analysis based on Lang's equations [13].

4.3.4 Analysis of optical and RF Spectra

In the numerical simulation, we have assumed three identical semiconductor lasers for one ML and two SLs in Fig. 4-12. It is assumed that the ML is modulated at 8 GHz so that the optical spectrum exhibits the ± 2 sideband power larger than the other sideband power in the optical spectrum, where the average ML power is of 3 mW. We have designated the ± 2 sidebands as target sidebands of two SLs, whose beat signal frequency is 32 GHz in the RF-spectrum. The ML output power passing through an optical attenuator is injected into two SLs as illustrated in Fig. 4-12. The adjustment of the ML bias level or the modulation power will change the IM / FM indexes deviating the whole optical spectrum, consequently. By controlling optical attenuator, the ML injection power can be adjusted with no deviation of the optical spectrum. We have investigated the effect of the unselected sidebands on the spectral characteristics for the different ML powers. In the numerical simulation, we have not considered the path length differences in the path to two SLs from ML and the path to PD from two SLs. The SL transient responses are solved by the fourth order Runge-Kutta integration of the field rate-equations in Eq. (4-10). Two SLs in Fig. 4-12 are both assumed biased at $1.96 \times I_{th}$, at which they emit the optical power of 5 mW in the free-running state. I_{th} is 33.5 mA, here. Then, one of the two SLs in Fig. 4-12 is frequency detuned to become locked to the +2 or, -2 target sideband for the different ML powers. The optical spectra of the locked SL can be obtained from the fast-

Fourier transformation (FFT) of the SL output power at the steady-state solution of the transient response.

Figure 4-14 shows the optical and RF-spectra of two SLs, which have the frequency separation of 32 GHz in the free-running state. In Fig. 4-14 (A), each SL has the positive (negative) frequency detuning by 16 GHz from the ML center frequency and its frequency in the free-running state agrees with the frequency of the +2 (or -2) target sideband. The optical power ratio between the ML average power and each free-running SL is of –17.2 dB, here. The desired beat signal at 32 GHz is little distinguishable. From Fig. 4-14 (A), the additional frequency-detuning offsets from the target sideband frequency are required for the stable locking due to the *R*-dependent asymmetry of the stable locking regime.
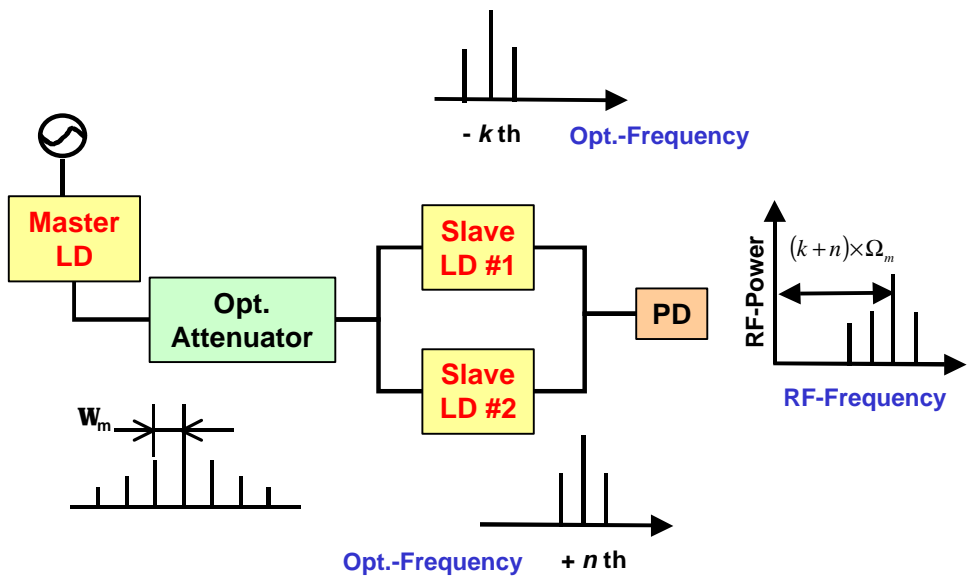
Fig. 4-12. Block diagram for the sidebands selection using optical injection locking
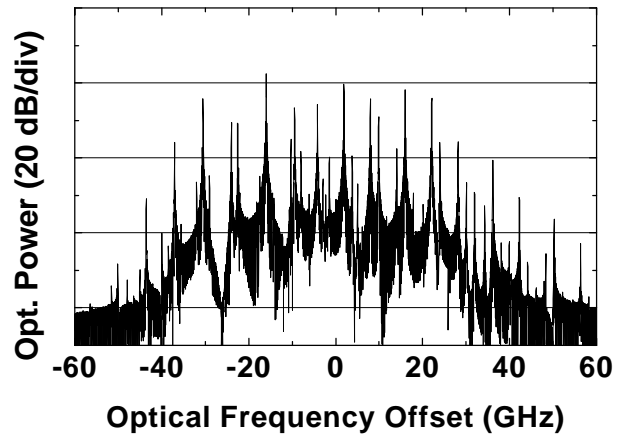
(a) Optical Spectra
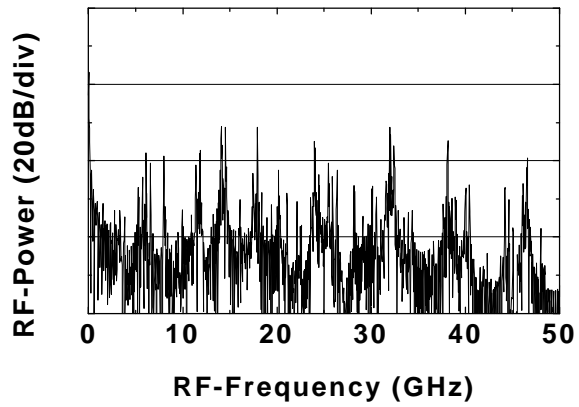
(b) RF-Spectrum

(A) Unlocked
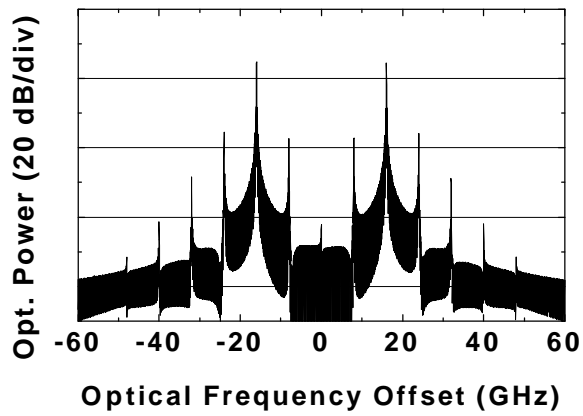
(a) Optical Spectra
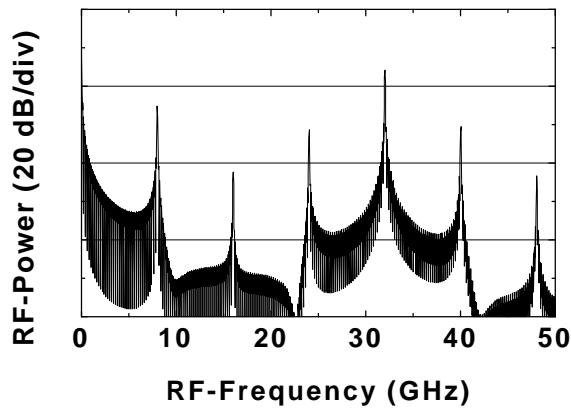
(b) RF-Spectrum

(B) Locked

Fig. 4-13. Optical and RF spectra of two SLs when both are (A) unlocked
and (B) locked

Figure 4-14 shows the optical and RF spectra when the additional detuning offsets (of -31 GHz, here) from the target sideband frequencies for the stable-locking are taken into account. The detuning offset, $\Delta\boldsymbol{n}_k$, for the k-th sideband locking is defined as

$$\Delta\boldsymbol{n}_k = f_k^{ML} - f_k^{SL} \tag{4-15}$$

where f_k^{ML} is the frequency of the ML k-th sideband. In the simulation, the same detuning offset of –31 GHz can be used since the ± 2-nd target ML sidebands have almost the same peak power in the optical spectrum. Unlike the unlocking case in Fig. 4-13, Figure 4-14 shows two locked peak powers in the optical spectrum having the desired frequency separation of 32 GHz. Consequently, the desired beat signal after PD can be obtained at 32 GHz in the RF spectrum.

One should note here that the optical spectrum exhibits the distinctive peaks beside two target sidebands. They are separated by the modulation frequency, 8 GHz. And, the RF spectrum also shows the unwanted RF power peaks beside the desired beat signal. We believe that these spectral behaviors are caused by the presence of the unselected ML sidebands in the selection of the target sidebands by the optical injection-locking method. When the target sideband and SL meet the stable-locking conditions, the optical power of the SL is shifted to the target sideband mode. Although the unselected sidebands do not meet the locking conditions, they will not cause any unlocking

characteristics since most of the SL power is contributed to the locking of the target sideband and then the unselected sidebands will not have enough optical gain to cause any unlocking characteristics. Consequently, the unselected sidebands will be amplified just a little with the depleted optical gain. Therefore, the unwanted powers in the optical and RF spectra due to the presence of the unselected sidebands will increase with the average ML powers with the multiple sidebands. The unwanted optical modes beside the target sideband modes may cause the chromatic dispersion problem in the fiber-optic transmission, and will degrade the overall system performance [6].

In order to suppress the unwanted optical modes at the unselected sidebands, the incident ML power into the SL shall be as small as possible. However, as shown in Fig. 4-14 (A), since the width of the stable locking regime is dependent upon power injected into ML, the smaller ML power injection will make a narrow in the stable locking regime. The narrow stable locking regime will cause the stability problems due to the operating current and temperature fluctuations. And, typically, the large modulation index is required for the better carrier-to-noise ratio (CNR). But, the large modulation depth is limited by the narrow stable-locking regime. For the larger modulation depth and better CNR, the broad stable-locking condition will be preferable. Then, the incident ML power should be increased as a trade-off.

Figure 4-14 shows the spectral characteristics for the power ratios of –37.2 dB and –7.2 dB. For the small R in Fig. 4-14 (A), the unwanted optical modes beside the target sideband mode are so greatly suppressed in the optical

domain that the beat signal at the desired frequency of 32 GHz is dominant in the RF-spectrum. However, for the relatively large R in Fig. 4-14 (B), the target sideband mode in the optical domain is still dominant, but the unwanted sideband modes are much less suppressed. Consequently, the unwanted beat signal powers become comparable to the desired beat signal power in the RF-spectrum and cannot be ignored. In order to select the desired beat signal in Fig. 4-14 (B), the electrical bandpass filters with the narrow bandwidth are needed. Two adjacent RF-powers beside the desired signal frequency will be of our major concern in the filter design. Figure. 4-15 shows the power difference (ΔP) between the desired signal power at 32 GHz (P_{32}) and one adjacent RF-power at 40 GHz (P_{40}) for the different power ratios (R's). If it is assumed that the adjacent power is to be suppressed by 20 dB in the filter design, the incident ML power should meet the power ratio of less than –20 dB.

Figure 4-16 shows the RF-spectrum when the ± 2nd target ML sidebands are used for the 32 GHz beat signal generation. P_n in the figure denotes the RF-power at n-GHz. Figure 4-16 shows the power difference (ΔP) between P_{32} and P_{40} when a variable attenuator with no deviation of the ML optical spectrum optically attenuates the incident ML power. The calculated ΔP is in good agreement with the measured results in Fig. 4-17 [66]. In Fig. 4-17, numerical simulation model and experimental results agree very well [66]. The difference is due to different operating points in measurement and model, omitted phase noise in the model, and inaccurate parameter values.
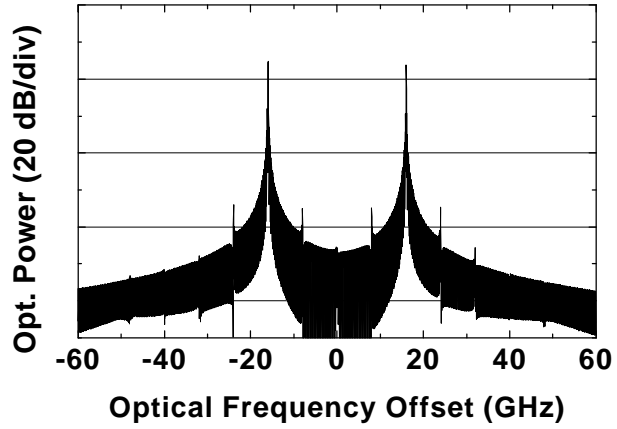
(a) Optical Spectra
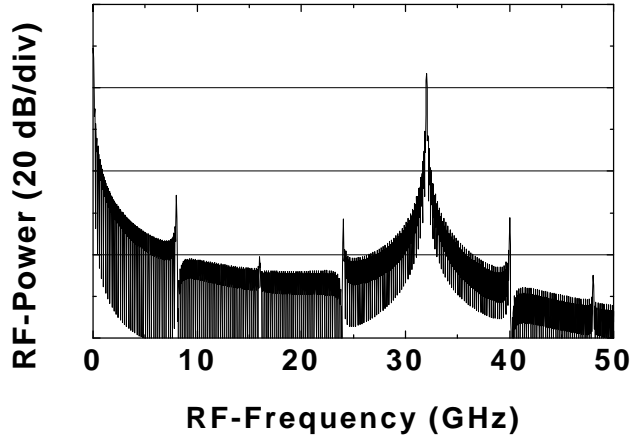
(b) RF-Spectrum

(A) R = -37.2 dB
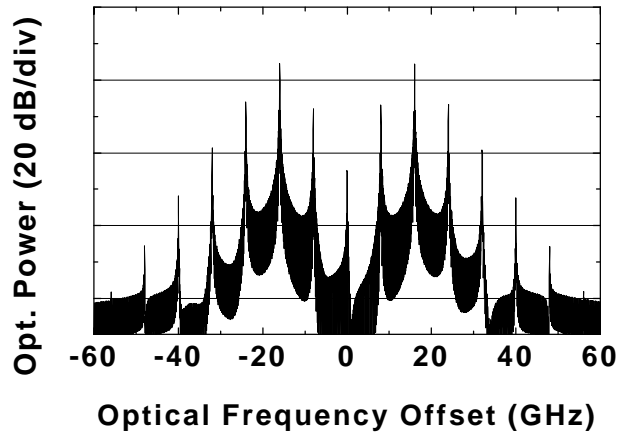
(a) Optical Spectra
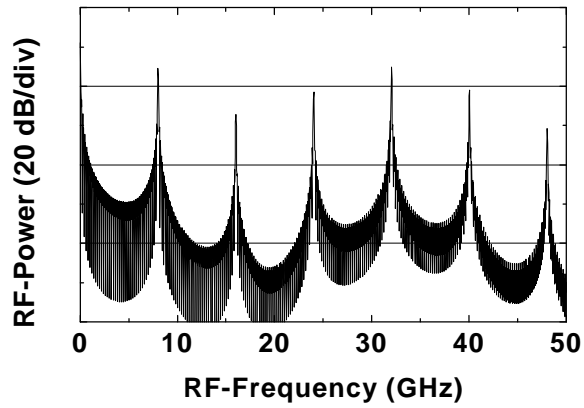
(b) RF-Spectrum

(B) R = -7.2 dB

Fig. 4-14. Spectral dependence for the different power ratios
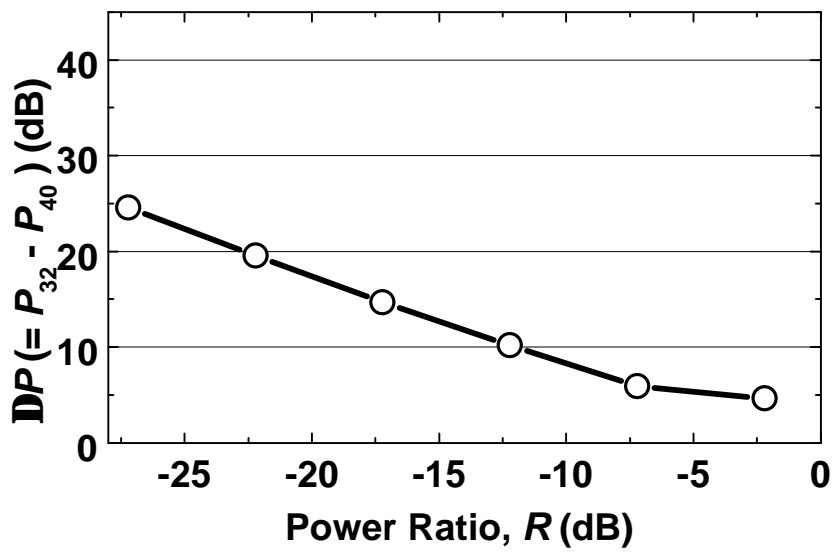
Fig. 4-15. Power difference between the RF powers at 32 GHz and 40 GHz
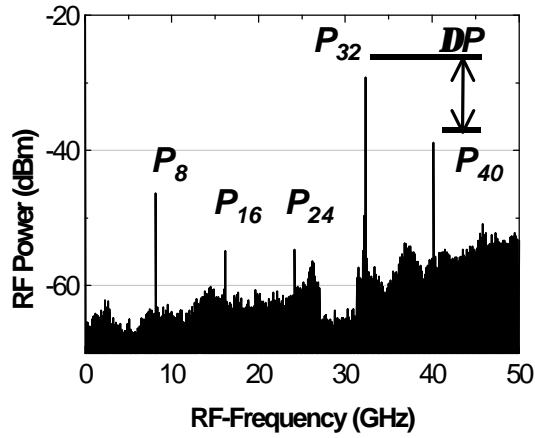
(a) RF-spectra
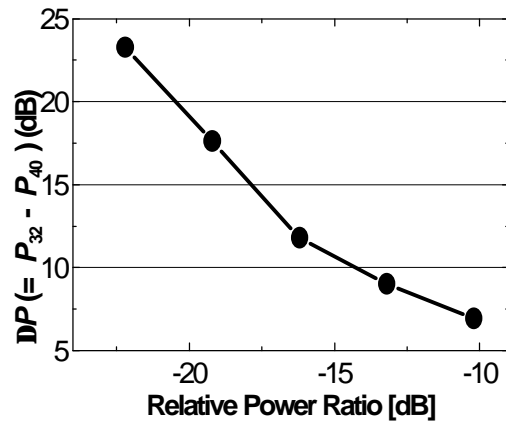
(b) Power difference

Fig. 4-16. (a) Measured RF-spectra in the 32 GHz beat signal generation

and (b) ΔP between P_{32} and P_{40} [66]
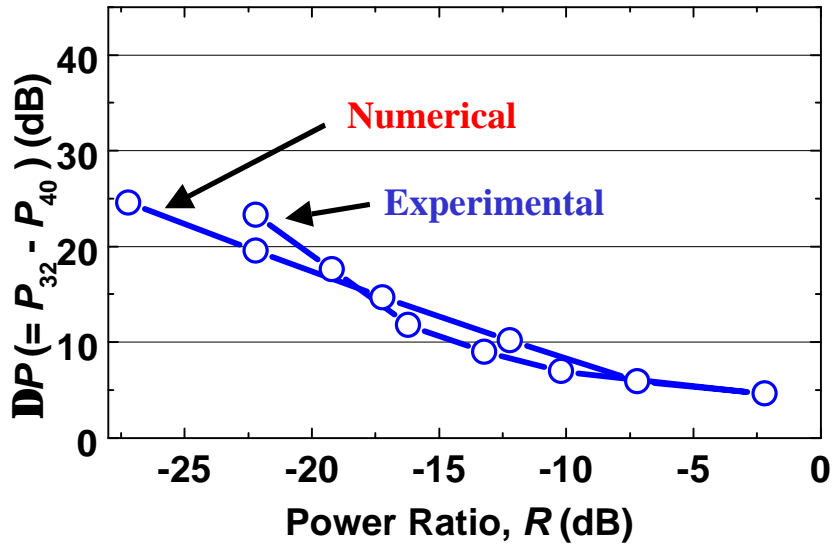
Fig. 4-17. Comparison of measured and calculated ΔP between P_{32} and P_{40}

Chapter 5. Conclusions

5.1 Summary

Microwave signals in cellular broad-band mobile communication networks and distributed networks can favorably be generated and distributed by optical techniques. In principle, these techniques have already been investigated for optical control of phase-array antennas, characterization of photodetectors and phase locking of millimeter-wave oscillators and now being applied to wireless communications. The generation and transmission of millimeter-wave radio signals by optical means is of special interest for future pico-cell broadband mobile communication systems, especially for systems operating at frequencies of 30 GHz. Prerequisites for the implementation of these systems are reliable low-cost components and technological principles. Here, the combination of light and millimeter-wave techniques is a promising solution. Since a laser diode and a photodiode are required for the optical feeder link between the control station and the base station, the millimeter-wave signal can be optically generated, offering a variety of advantages including a cost reduction due to the fact that no millimeter-wave oscillators and modulators are necessary in the numerous base stations.

The combination of fiber optics and millimeter-wave techniques offers advantages for pico-cell broadband mobile communication systems. Addition to the low-loss transmission and large bandwidth of the fibers, the remote

generation of the millimeter-wave signals is a powerful advantage of the optical technique. In this dissertation, experiments on generating millimeter-wave signals by optical injection locking method have been investigated.

In conclusion, we have investigated the spectral characteristics of the semiconductor lasers locked to the sidebands of the master laser, which were expressed by a series of the Bessel function. The numerical model for the semiconductor lasers based on the typical Lang's equation has been extended in order to take into account the simultaneous injection of the multiple sidebands of the directly modulated ML. The numerical simulations have showed that the unselected sidebands can affect the optical and RF-spectral characteristics even when the semiconductor laser is stable-locked to the target sidebands. Due to the presence of the unselected sidebands, the unwanted powers in the optical and RF-spectra will increase with the ML power, and be combined with the fiber chromatic dispersion so that they may degrade the overall system performance. We have found that the simulation results are in good agreement with the experimental results [66].

5.2 Future Research Directions

In future radio communications, many users will desire to handle multimedia with high quality. A millimeter-wave is expected to be a promising and important frequency for future radio communication systems. Figure 1-1 shows the generic architecture of the fiber-optic millimeter-wave radio access

network. It consists of a control station, a fiber-optic access network, base station's and millimeter-wave wireless terminals in pico-cells and indoor wireless local area networks. The control station has the optical transceiver that controls and converts the signals between fiber-optic networks. The base station, which is an access point for the wireless terminal's, has the optic-to-electric and electric-to-optic converts with a millimeter-wave antenna, for the downlink and the uplink, respectively. We will investigate on the fiber-optic downlink system for distributing 30 GHz band millimeter-wave signals from control station to base station. In consideration of system, we have to estimate optical part and electrical part. First of all, we will investigate the optical link and make a data format to estimate system performance numerically. Second, we will extract parameters to estimate fiber-optic system performance.

References

[1] Zaheer Ahmed, Dalma Novak, and Hai-Feng Liu, "37 GHz fiber-wireless systems for distribution of broad-band signals," *IEEE Trans. Microwave Theory and Techniques*, Vol. 45, No. 8, pp. 1431-1435, August 1997.

[2] Xue Jun Meng, Dennis T. K. Tong, and Ming C. Wu, "Demonstration of an analog fiber-optic link employing a directly modulated semiconductor laser with external light injection," *IEEE Photon. Technol. Lett.,* Vol. 10, No. 11, pp. 1620-1622, November 1998.

[3] Junn-Shyen Wu and Hen-Wai, "A radio over fiber network for microcellular system application," *IEEE Trans. on Vehicular Technology*, Vol. 47, No. 1, pp. 84-94, February 1998.

[4] J. M. Liu, Chen. X. J, and T. B. Simpson, "Modulation bandwidth, noise, and stability of a semiconductor laser subject to strong injection locking," *IEEE Photon. Technol. Lett.,*, Vol. 9, No. 15, pp. 1325-1327, October 1997.

[5] M. Gagnaire, "An overview of broad-band access technologies," *Proc. of IEEE*, Vol. 85, No. 12, pp. 1958-1972, 1997.

[6] U. Gliese, S. Naskov, and N. Nielsen, "Chromatic dispersion in fiber-optic microwave and millimeter-wave links," *IEEE Trans. Microwave Theory and Techniques*, Vol. 44, No. 10, pp. 1716-1724, 1996.

[7] U. Gliese, S. N. Nielsen, and T. N. Nielsen, "Limitations in distance and frequency due to chromatic dispersion in fiber-optic microwave and

millimeter-wave links," *1996 IEEE MTT-S Digest*, pp. 1547-1550.

[8] F. Ramos, J. Marti, and J. M. Fuster, "On the use of fiber-induced self-phase modulation to reduce chromatic dispersion effects in microwave/millimeter-wave optical systems," *IEEE Photon. Technol. Lett.*, Vol. 10, No. 10, pp. 1473-1475, October 1998.

[9] V. Etten and V. D. Plaats, *Fundamentals of Optical Fiber Communications*, Prentice Hall, 1991.

[10] R. P. Braun, G. Grosskopf, D. Rohde, F. Schmidt, and G. Walf, "Fiber-optic millimeter-wave generation at 64 GHz and spectral efficient data transmission for mobile communications," in Tech. Dig. *Optical Fiber Communications Conference (OFC98)*, TuC4, pp. 17-18, 1998.

[11] G. P. Agrawal, *Fiber-optic Communication Systems*, John Willy & Sons, INC,1992.

[12] G. H. Smith, D. Novak, C. Lim, and K. Wu, "Technique for optical SSB generation to overcome dispersion penalties in fiber-radio systems," *Electron. Lett.*, Vol. 33, No. 1, pp. 74-75, 1997.

[13] G. H. Smith, D. Novak, and Z. Ahmed, "Overcoming chromatic-dispersion effects in fiber-wireless systems incorporating external modulators," *IEEE Trans. Microwave Theory and Techniques*, Vol. 45, No. 8, pp. 1410-1415, 1997.

[14] Leonid Kazovsky, *Optical Fiber Communication Systems*, Artech House, 1996.

[15] Andreas Stohr, Ken-ichi Kitayama, and Dieter Jager, "Full-duplex fiber-

optic RF subcarrier transmission using a dual-function modulator/photodetector," *IEEE Trans. Microwave Theory and Techniques*, Vol. 47, No. 7, pp. 1338-1341, July 1999.

[16] F. Ramos, J. Marti, and V. Polo, "Compensation of chromatic dispersion effects in microwave/millimeter-wave optical systems using four-wave-mixing induced in dispersion-shifted fibers", *IEEE Photon. Technol. Lett.*, Vol. 11, No. 9, pp. 1171-1173, September 1999.

[17] X. L. Wang, H. Yokoyama, and T. Shimizu, "Synchronized harmonic frequency mode-locking with laser diodes through optical pulse train injection," *IEEE Photon. Technol. Lett.*, Vol. 8, No. 5, pp. 617-619, 1996.

[18] Clemens H, Von Helmolt, Udo Kruger, Kirsten Kruger, and Gerd Grosskopf, "A mobile broad-band communicaiton system based on mode-locked lasers," *IEEE Trans. Microwave Theory and Techniques*, Vol. 45, No. 8, pp. 1424-1430, August 1997.

[19] L. Noel, D. Wake, and D. Nesset, "Novel techniques for high-capacity 60 GHz fiber-radio transmission systems," *IEEE Trans. Microwave Theory and Techniques*, Vol. 45, No. 8, pp. 1416-1423, August 1997.

[20] E. Hashimoto, A. Takada, and Y. Katagiri, "Synchronization of sub-terahertz optical pulse train from PLL-controlled colliding pulse mode-locked semiconductor laser," *Electron. Lett.*, Vol. 34, No. 6, pp. 580-581, 1998.

[21] L. N. Langley, M. O. Elkin, C. Edge, M. J. Wale, U. Gliese, X. Huang, and A. J. Seeds, "Packaged semiconductor laser optical phase-locked

loop (OPLL) for photonic generation, processing and transmission of microwave signals," *IEEE Trans. Microwave Theory and Techniques*, Vol. 47, No. 7, pp. 1257-1264, 1999.

[22] J. C. Cartledge and G. S. Burley, "The effect of laser chirping on lightwave system performance," *J. Lightwave Technol.*, Vol. 7, pp. 568-573, 1989.

[23] L. Noel, D. Marcenanc, and D. Wake, "Optical millimeter-wave generation technique with high efficiency, purity, and stability," *Electron. Lett.*, Vol. 32, No. 21, pp. 1997-1998, 1996.

[24] L. Goldberg, H. F. Taylor, and J. F. Weller, "Microwave signal generation with injection-locked laser diodes," *Electron. Lett.*, Vol. 19, No. 13, pp. 491-493, 1983.

[25] R. P. Braun, G. Grosskopf, R. Meschenmoser, D. Rohde, F. Schmidt, and G.Villino, "Microwave generation for bidirectional broadband mobile communications using optical sideband injection locking,*" Electron. Lett.*, Vol. 33, No. 16, pp. 1395-1396, 1997.

[26] C. H. Lange, J. Eom, and C. B. Su, "Measurement of intrinsic frequency response of semiconductor lasers using optical modulation," *Electron. Lett.*, Vol. 24, pp. 1132-1132, 1988.

[27] C. Lin and F. Mengel, "Reduction of frequency chirping and dynamic linewidth in high-speed directly modulated semiconductor lasers by injection locking," *Electron. Lett.,* Vol. 20, pp. 1073-1075, 1984.

[28] C. B. Su, J. Eom, C. H. Lange, C. B. Kim, R. B. Lauer, W. C. Rideout,

and J. S. LaCourse, "Characterization of the dynamics of semiconductor lasers using optical modulation," *IEEE J. Quant. Electron.*, Vol. 28, pp. 118-127, 1992.

[29] K. Inoue and N. Takato, "Wavelength conversion for FM light using light injection induced frequency shift in DFB-LD," *Electron. Lett.*, Vol. 25, pp. 1360-1362, 1989.

[30] L. Goldberg, H. F. Taylor, and J. F. Weller, "FM sideband injection of diode lasers," *Electron. Lett.,* Vol. 18, pp. 1019-1020, 1982.

[31] R.P. Braun, G. Grosskopf, D. Rohde, F. Schemidt, and G. Walf, "Fiber-optic millimeter-wave generation at 64 GHz and spectral efficient data transmission for mobile communications," *OFC' 98*, pp. 17-18, 1998.

[32] U. Gliese, T. Nørskov, and K. E. Stubkjær, "Multifunctional fiber-optic microwave links based on remote heterodyne detection," *IEEE Trans. Microwave Theory and Technology*, Vol. 46, pp. 458-468, 1998.

[33] R.P. Braun, "Fiber Radio Systems, Applications and Devices," in Tutorial *European Conferenece on Optical Communication (ECOC'98)*, Vol. 2, pp. 87-119, 1998.

[34] O. Lidoyne, P. B. Gallion, and D. Erasme, "Modulation properties of an injection-locked semiconductor laser," *IEEE J. Quant. Electron.*, Vol. 27, pp. 344-351, 1991.

[35] S. Kobayashi, Y. Yamamoto, and T. Kimura, "Direct frequency modulation in AlGaAs semiconductor lasers," *IEEE J. Quant. Electron.*, Vol. 18, pp. 582-595, 1982.

[36] Toshiaki Kuri, Ken-ichi Kitayama, and Yasunori Ogawa, "Fiber-optic millimeter-wave uplink system incorporating remotely fed 60 GHz band optical pilot tone," *IEEE Trans. Microwave Theory and Technology*, Vol. 47, no. 7, pp. 1332-1337, July 1999.

[37] Toshiaki Kuri, Ken-ichi Kitayama, and Yoshiro Takahashi, "Simplified BS without light source and RF local oscillator in full-duplex millimeter-wave radio-on-fiber system based upon external modulation technique," *MWP' 99 Digest*, pp. 123-126.

[38] G. P. Agrawal, "Power spectrum of directly modulated single-mode semiconductor lasers : chirp-induced fine structure," *IEEE J. Quant. Electron.*, Vol. 21, No. 6, pp. 680-686, 1985.

[39] R. Lang, "Injection locking properties of a semiconductor laser," *IEEE J. Quant. Electron.*, Vol. QE-18, No. 6, pp. 976-983, 1982.

[40] Biswanath Mukherjee, *Optical Communicaiton Networks*, McGraw-Hill, 1997

[41] J. Wang, M. K. Haldar, and F. V. C. Mendis, "Enhancement of modulation bandwidth of laser diodes by injection locking," *IEEE Photon. Technol. Lett.*, Vol. 8, No. 1, pp. 34-36, January 1996.

[42] T. B. Simpson and J. M. Liu, "Enhanced modulation bandwidth in injection-locked semiconductor lasers," *IEEE Photon. Technol. Lett.*, Vol. 9, No. 10, pp. 1322-1324, October 1997.

[43] Powers, *An Introduction to Fiber Optic Systems*, Aksen Associates, 1993.

[44] Gnitaboure Yabre, "Improved direct-modulation characteristics of a

semiconductor laser by FM/IM conversion through an interferometer,"
J. Lightwave Technol., Vol. 14, No. 10, pp. 2135-2140, 1996.

[45] Gnitaboure Yabre, "Effect of relatively strong light injection on the chirp-to-power ratio and the 3 dB bandwidth of directly modulated semiconductor lasers," *J. Lightwave Technol.*, Vol. 14, No. 10, pp. 2367-2373, October 1996.

[46] Gnitaboure Yabre and Jean Le Bihan, "Reduction of nonlinear distortion in directly modulated semiconductor lasers by coherent light injection," *IEEE J. Quant. Electron.*, Vol. 33, No. 7, pp. 1132-1140, July 1997.

[47] J. Le Bihan and G. Yabre, "FM and IM intermodulation distortions in directly modulated single-mode semiconductor lasers," *IEEE J. Quant. Electron.*, Vol. 40, No. 40, pp. 899-904, April 1994.

[48] Linlin Li and Klaus Petermann, "Small-signal analysis of optical-frequency conversion in an injection-locked semiconductor laser," *IEEE J. Quant. Electron.*, Vol. 30, No. 1, pp. 43-48, June 1991.

[49] Masahiro Tsuchiya and Takeshi Hoshida, "Nonlinear photodetection scheme and its system applications to fiber-optic millimeter-wave wireless down-links," *IEEE Trans. Microwave Theory and Technology*, Vol. 47, No. 7, pp. 1342-1350, July 1999.

[50] Stephen Bennett, Christopher, and Stavros Iezekiel, "Nonlinear dynamics in directly modulated multiple quantum well laser dioses," *IEEE J. Quant. Electron.*, Vol. 33, No. 11, pp. 2076-2083, November 1997.

[51] F. Mogensen, H. Olesen, and G. Jacobsen, "Locking conditions and

stability properties for a semiconductor laser with external light injection," *IEEE J. Quant. Electron.*, Vol. QE-21, No. 7, pp. 784-793, 1985.

[52] Xue Jun Meng, Tai Chau, and Ming C. Wu, "Improved intrinsic dynamic distortions in directly modulated semiconductor lasers by optical injection locking," *IEEE Trans. Microwave Theory and Technology*, Vol. 47, No. 7, pp. 1172-1176, July 1999.

[53] Yang Jing Wen, Hai Feng Liu, and Dalama Novak, "Millimeter-wave signal generation from a monolithic semiconductor laser via subharmonic optical injection," *IEEE Photon. Technol. Lett*, Vol. 12, no. 8, pp. 1058-1060, August 1993.

[54] O. Lidoyne, P. Gallion, C. Chabran, and G. Debarge, "Locking range, phase noise and power spectrum of an injection-locked semiconductor laser," *IEE Proceedings*, Vol. 137, No. 3, pp. 147-154, 1990.

[55] K. Kikuchi, C.E. Zah, and T.P. Lee, "Amplitude-modulation sideband injection locking characteristics of semiconductor lasers and their application," *J. Lightwave Technology*, Vol. 6, No. 12, pp. 1821-1830, 1988.

[56] J. Wang, M. K. Haldar, L. Li, and F. V. C. Mendis, "Enhancement of Modulation Bandwidth of Laser Diodes by Injection Locking," *IEEE Photon. Technol. Lett.*, Vol. 8, No. 1, pp. 34-36, 1996.

[57] T. B. Simpson, M. Liu, and A. Gavrieldides, "Bandwidth enhancement and broadband noise reduction in injection-locked semiconductor

Lasers," *IEEE Photon. Technol. Lett.*, Vol. 7, No. 7, pp. 709-711, 1995.

[58] V. Kovanis and A. Gavrielides, "Instabilities and chaos in optically injected semiconductor lasers," *Appl. Phys. Lett.*, Vol. 67, No. 19, pp. 2780-2782, 1995.

[59] E. Peral *et al.*, "Large-signal theory of the effect of dispersive propagation on the intensity modulation response of semiconductor lasers," *J. Lightwave Technol.*, Vol. 18, pp. 84-89, 2000.

[60] M. D. Pelusi, H. F. Liu, and Y. Ogawa, "THz optical beat frequency generation from a single mode locked semiconductor laser", *Appl. Phys. Lett.*, Vol. 71, No. 4, pp. 449-451, 1997.

[61] Paul E. Green, Jr. *Fiber Optic Networks*, Prentice Hall, 1993.

[62] G.H.Smith and D. Novak, "Broadband millimeter-wave fiber-radio network incorporating remote up/downconversion", *IEEE MTT-S Digest*, pp. 1509-1512, 1998.

[63] K. Yonenaga and N. Takachio, "A fiber chromatic dispersion compensation technique with an optical SSB transmission optical homodyne detection systems," *IEEE Photon. Technol. Lett.*, Vol. 5, pp. 949-951, 1993.

[64] Mark S. Leeson, "Performance Analysis of direct detection spectrally sliced receivers using fabry-perot filters," *J. Lightwave Technol.*, Vol. 18, No. 1, pp. 13-25, January 2000.

[65] J.T. Kim, *et al.*, "Optical generation of millimeter-waves using injection-locked four-wave-mixing modes in semiconductor lasers," *The Second*

Korea-Japan Joint Workshop on Microwave-photonics, Technical Digest, pp. 137-140, February 2001.

[66] Jung-Tae Kim *et al.*, "Spectral characteristics of semiconductor lasers locked to external light injection from a current-modulated laser," *SPIE's Optoelectronics 2001*, pp. 54-55, January 2001.

[67] J.T. Kim, "Analysis of performance employing chromatic dispersion," TE25, pp.153-154, *Photonics conference 2000*.

[68] J.T. Kim *et al.*, "Optical millimeter-wave generation using injection-locking scheme," *IEEE MTT/AP/EMC Korea Chapter*. pp. 171-174, 2000.

[69] J.T, Kim, "Performance Analysis of Broadband System Employing Fiber-optic Links," TE26, pp. 156-157, *Photonics conference 1999*.

[70] R. A. Griffin, P. M. Lane, and J. J. O' Reilly, "Dispersion-tolerant subcarrier data modulation of optical millimeter-wave signals," *Electron. Lett*., Vol. 32, No. 24, pp. 2258-2260, November 1996.

[71] J. Troger, P.A. Nicati, L. Thevenaz, and P. A. Robert, "Novel measurement scheme for injection-locking experiments," *IEEE J. Quant. Electron*., Vol. 35, pp. 32-38, 1999.

[72] J.T.Kim *et al*., "Optical Generation of Microwave Signals Using a Directly Modulated Semiconductor Laser under Modulated Light Injection," *Microwave and Optical Technology Letters*, Vol. 30, No. 6, September 2001.

[73] Silvello Betti et al., *Coherent Optical Communications Systems*, John Willey & Sons, INC, 1995

,

.   ,

.   ,

.

xDSL (x-Digital

Subscriber Line)   HFC (Hybrid Fiber Coaxial)   ,

WITL (Wireless In The

Loop)   FITL (Fiber In The Loop)   .

WITL

. WITL

BWLL (Broadband Wireless Local Loop), LMDS (Local

Multipoint Distribution System), MBS (Mobile Broadband Systems)   .

,

30 GHz   BWLL   .

LAN,   Intelligent

Transportation System,

.

,

, Sideband injection locking

.

Optical injection locking   sub-

harmonic   RF source   ,

sideband

RF   .

,   sideband

sideband

lock   , PD   .

,   sideband

injection-locking   sideband   beat signal

.   beat signal

,

.   ,   beat signal

, 30 GHz

.

_____